ФИЗИКА ЭЛЕМЕНТАРНЫХ ЧАСТИЦ И АТОМНОГО ЯДРА. ТЕОРИЯ

SOLAR NEUTRINOS. ASTROPHYSICAL ASPECTS

V. A. Naumov [1]

Joint Institute for Nuclear Research, Dubna

This paper is a short pedagogical introduction to some aspects of the solar neutrino problem. The basic attention is concentrated on a qualitative consideration of the pp and CNO reactions responsible for hydrogen burning in the Sun, starting from an elementary derivation of the formula for the nonresonant thermonuclear reaction rate. We outline the physical content of the standard solar models, the problem of chemical composition of the Sun, expected neutrino energy spectrum, radial distributions of the neutrino fluxes in the Sun, and uncertainties in the predicted neutrino event rates.

Статья представляет собой краткое педагогическое введение в проблему солнечных нейтрино. Основное внимание сосредоточено на качественном рассмотрении pp- и CNO-реакций, отвечающих за процесс горения водорода в Солнце, начиная с элементарного вывода формулы для скоростей нерезонансных термоядерных реакций. Обсуждаются физические принципы, заложенные в основу стандартных солнечных моделей, проблема химического состава Солнца, ожидаемый энергетический спектр солнечных нейтрино, радиальные распределения потоков нейтрино в Солнце, неопределенности в предсказаниях скорости счета нейтринных событий.

PACS: 26.65.-t; 96.60.-j; 96.60.Fs; 96.60.Jw; 96.60.Ly; 26.20.Cd

INTRODUCTION

The life of any star is an unceasing struggle between gravity and pressure. Gravity tries to compress everything to the star's core. Pressure acts in all directions, but decreases with increasing distance from the core, thus pushing stellar layers outward. When gravity dominates, the star contracts causing the pressure to rise and thus resisting further contraction. When the outward pressure gradient dominates, stellar layers expand, thus decreasing the pressure and terminating further expansion. Since a star shines, it loses energy from its interior. This reduces the pressure and leads to contraction of the star. Without a mechanism of restoring the energy lost, a typical star cannot live more than some tens of millions of years. It has long been known that such a mechanism is provided by the reactions of thermonuclear fusion (the formation of light nuclei from lighter ones) within the star [2].

If the daughter nucleus is more bound than the fusing ones, the reaction releases nuclear binding energy. The latter rises steeply from zero for ^{1}H to about 7.07 MeV per nucleon for ^{4}He and reaches a peak at about 8.79 MeV per nucleon for the iron-nickel group (^{56}Fe, ^{58}Fe, ^{62}Ni) before decreasing for heavier nuclei. If a star initially consisted of pure hydrogen, it could gain a maximum of about 8.79 MeV per nucleon by fusion to iron or nickel. This

[1] E-mail: vnaumov@theor.jinr.ru
[2] This source of stellar energy has been originally suggested by Eddington [1] and Perrin [2] in 1920.

is an extremely complicated and multistage process occurring at very high temperatures and densities. But most of the available nuclear binding energy ($\sim 80\%$) is already released when ^{4}He is built up in the first stage. This stage is the fully dominant energy source for the present-day Sun. The energy production rate averaged over the solar core does not catch our fancy: it is as low as ~ 15 W/m^3. However, the luminosity of the Sun is about $4 \cdot 10^{26}$ W, equivalent to $\sim 10^{17}$ typical nuclear power plants. It is so huge because the Sun converts $\sim 7 \cdot 10^8$ metric tons of hydrogen to helium per second. The hydrogen is consumed at a lower rate than in any other evolutionary phase of the Sun and thus the central H-burning lifetime of the Sun is longer than that for other phases. The Sun contains $\sim 10^{57}$ atoms (mostly hydrogen); so it has enough fuel to shine actively for more than 10^{10} y.

A conversion of a proton into a bound neutron is only possible with production of an electron neutrino through β^+ decay or electron capture. The hydrogen-to-helium fusion is also a rather multistage process which occurs in two key simultaneously running reaction sequences, the pp (or proton–proton) chains and the CNO (Carbon–Nitrogen–Oxygen) cycle [1] and the electron neutrinos are necessarily emitted as a result of some of the pp and CNO reactions. Since these low-energy neutrinos are extremely penetrating ultrarelativistic particles, they escape the Sun in two seconds and reach the Earth in about eight minutes from the time they were produced. By detecting the «solar» neutrinos, we may learn a lot about the «instantaneous» physical conditions inside the Sun and, as a surprising bonus, about the neutrinos themselves.

The solar neutrinos were investigated in order to prove that the Sun is actually powered by thermonuclear fusion. In 1965, Davis and his team began construction of the chlorine solar neutrino experiment in the Homestake Gold Mine at Lead, South Dakota. According to the data published in 1968 [5], the detector count rate was substantially smaller than the solar models of the day predicted [6]. That was the first indication of the so-called «solar neutrino problem», which has been confirmed by almost 25 years of the Homestake detector operation and by several further solar neutrino experiments relying on different detection methods. This gave rise to a number of investigations and worthwhile ideas — some of which are still alive.

Now, after more than forty years of intense multidisciplinary efforts it seems that the long-standing solar neutrino problem is basically resolved. At least, it is widely believed that the modern solar neutrino experiments and helioseismic observations, together with complementary experimental and theoretical studies, have proven that the Sun shines due to nuclear fusion, while the observed neutrino deficit is explained by neutrino oscillation phenomenon, as a consequence of finite neutrino masses and flavor mixing [2].

This article is an introductory overview (meant for nonspecialists) to some astrophysical aspects of the solar neutrino problem. It is primarily focused on a qualitative consideration of the pp and CNO reactions in the Sun. Because of the limited volume of the article, it does not touch upon the results of the solar neutrino experiments and the status of the various solutions to the solar neutrino anomalies. While these items are crucial for understanding the solar neutrino problem, they are postponed to another paper. The interested reader is referred to comprehensive recent reviews and monographs (see, e.g., [8–10] and references therein).

---

[1]Both sequences were worked out at the end of the 1930s [3,4], though without mentioning the neutrinos.

[2]It should be noted that the hypothesis of neutrino mixing was put forward by Pontecorvo in 1957 [7] that is long before the solar neutrino problem has been recognized.

1. THE SUN IS A RELATIVISTIC MACHINE

Hereby the net fusion reaction in the Sun is burning hydrogen to make helium:

$$4\,^1\mathrm{H} \rightarrow \,^4\mathrm{He} + 2e^+ + 2\nu_e. \tag{1}$$

This reaction is written taking into account the constraints of conservation of electric charge, baryon and lepton numbers. The final helium nucleus has less internal energy than the initial hydrogen nuclei. This is a purely relativistic effect. Since energy is conserved, extra heat is released as energy of motion of the secondary particles and production of photons and neutrinos. Several γ quanta are created in the various steps of the net reaction (1), including e^+e^- annihilation; they are then degraded due to absorption by the solar plasma and reemission into many low-energy photons having the same total energy. The neutrinos promptly shoot out of the Sun, taking away a few percent of the produced energy. As a result, the solar plasma gets hotter and is enriched with lots of photons [1]. The energy release is

$$Q \approx (4 \cdot 1.007825u - 4.002603u) \cdot 931.5 \text{ MeV}/u \approx 26.732 \text{ MeV}$$

each time the reaction (1) happens. Here $1.007825u$ and $4.002603u$ are the masses of the hydrogen and helium atoms, respectively, and $u = (1/12)m(^{12}\mathrm{C}) \approx 1.660539 \cdot 10^{-27}$ kg ≈ 931.494 MeV is the unified atomic mass unit ($N_A u = 1$ g). This is a very efficient mechanism of energy generation. Although the obtained amount of energy corresponds only to about 0.7% of the relativistic mass defect, it is almost an order of magnitude larger than that produced in any other nuclear reaction process occurring in stars.

2. THE SUN IS A QUANTUM MACHINE

The fusion reaction (1) is, of course, a summary and may occur only in several steps, because the temperature and density in the Sun are too low. Moreover, from the point of view of classical physics, the temperature is so low that an inelastic collision of even *two* nuclei in the Sun is *nearly impossible*, since the amount of thermal energy, even in the core of the Sun, is not enough to overcome electric repulsion between the nuclei. Let us illustrate this statement quantitatively. The two nuclei have to get within $r_p \sim 10^{-13}$ cm for the strong interactions to hold them together. But the nuclei repel each other. For example, the Coulomb potential between two protons is $U = e^2/r_p \approx 2 \cdot 10^{-6}$ erg $\approx$ 1.2 MeV. Since $T_\odot \lesssim 1.5 \cdot 10^7$ K (the helioseismology confirms this), $\langle E_p^{\mathrm{kin}} \rangle = (3/2)kT_\odot \lesssim 2$ keV. Then by assuming Maxwell–Boltzmann distribution, the fraction of protons with $E_p^{\mathrm{kin}} > U$ is $\exp\left(-E_p^{\mathrm{kin}}/\langle E_p^{\mathrm{kin}} \rangle\right) < e^{-600} \sim 10^{-260}$. Remembering that the number of protons in the whole Sun is about 10^{57}, we can conclude that *the classical probability of the fusion is practically zero*. An explanation of why the fusion reactions in stars nevertheless occur was suggested in 1929 by Atkinson and Houtermans [11]. It is based on the quantum tunneling effect, developed earlier by Gamow [12] and independently by Gurney and Condon [13] in connection with the theory of α decay.

---

[1]Visible light photons leave the Sun after $\sim 10^5$ y and $\sim 10^{22}$ absorptions and reemissions.

Let us estimate the quantum probability for two nuclei to collide[1]. The wave function of a nonrotating nucleus a can be written in the quasi-classical approximation:

$$\psi \propto \exp\left(i \int p(r)dr\right) = \exp\left(i \int \sqrt{2m_a\left[E - U(r)\right]}dr\right).$$

Here and below we use the natural units, $\hbar = c = 1$. The repulsion energy of two nuclei with charges $Z_a e$ and $Z_b e$ is $U = Z_a Z_b \alpha / r$ (where $\alpha = e^2/\hbar c = e^2$). The classical turning point $(p(r) = 0)$ is given by $r_1 = Z_a Z_b \alpha / E$ and the momentum $p(r)$ is purely imaginary for $r < r_1$. Thus, the probability of the barrier penetration can be estimated (up to a normalization) as

$$\psi^2(r) \propto \exp\left[-2 \int\limits_{r_0}^{r_1} \sqrt{2m_a\left[U(r) - E\right]}\ dr\right],$$

where $r_0 \sim r_p$ is the radius of nuclear interaction. It has been implicitly assumed here that the second nucleus b is in rest. To avoid this assumption, one has to replace $m_a \approx A_a m_p$ with the reduced mass of the colliding nuclei:

$$m_a \longmapsto \mu = \frac{m_a m_b}{m_a + m_b} \equiv A m_p, \quad A \approx \frac{A_a A_b}{A_a + A_b}, \quad 1/2 \leqslant A < 1.$$

Considering that $r_p \sim 10^{-3} r_1$, we may put $r_0 = 0$ as a rough but reasonable approximation. Then the barrier penetration probability is estimated to be

$$\psi^2(r) \approx \psi^2(0) \propto e^{-2\pi\eta(E)}, \tag{2}$$

where

$$\eta(E) = \frac{r_1\sqrt{2\mu E}}{\pi} \int\limits_0^1 \sqrt{\frac{1}{x} - 1}\ dx = r_1\sqrt{\frac{\mu E}{2}} = \frac{1}{2\pi}\sqrt{\frac{E_G}{E}} \tag{3}$$

and

$$E_G = 2\left(\pi\alpha Z_a Z_b\right)^2 \mu. \tag{4}$$

The quantities (2), (3) and (4) are usually called the Gamow factor, Sommerfeld parameter and Gamow energy, respectively.

3. REACTION RATE

Let n_a be the number of nuclei $a = (A_a, Z_a)$ per unit volume in the solar plasma. In (assumed) thermal equilibrium with the temperature T the nonrelativistic particles obey the Maxwellian distribution over velocities, $n_a f(v_a)d\mathbf{v}_a$, where

$$f(v_a) = \left(\frac{m_a}{2\pi kT}\right)^{3/2} \exp\left(-\frac{m_a v_a^2}{2kT}\right) \text{ and } \int f(|\mathbf{v}|)d\mathbf{v} = 4\pi \int\limits_0^\infty f(v)v^2 dv = 1.$$

---

[1]Here we partially follow the simplified approach by Zeldovich et al. [14]. It neglects many essential details, in particular the electrostatic and dynamic screening effects in the solar plasma which generally lead to an enhancement of the nuclear reaction rates relative to those in vacuum.

Most of the nuclear reactions in stars are two-particle collisions which produce a set of other particles. The mean number of reactions $a + b \rightarrow c + \ldots$ per units of volume and time (the mean reaction rate) is given by

$$R_{a+b \rightarrow c+\ldots} = n_a n_b \langle \sigma_{ab}(v) v \rangle,$$

where $\sigma_{ab}(v) \equiv \sigma_{a+b \rightarrow c+\ldots}(v)$ is the reaction cross section, which depends on the relative velocity of the colliding particles $v = |\mathbf{v}_a - \mathbf{v}_b|$, and

$$\langle \sigma_{ab}(v) v \rangle = \int \sigma_{ab}(v) v f(v_a) f(v_b) d\mathbf{v}_a d\mathbf{v}_b = 4\pi \int_0^\infty \sigma_{ab}(v) v^3 f(v)\, dv. \tag{5}$$

The major difficulty in the calculation of the nuclear reaction rates of astrophysics interest is to determine the cross sections $\sigma_{ab}(v)$. Due to the exponential behaviour for the Coulomb tunneling, the cross section of the charged-particle induced nuclear reactions drops rapidly for the energies well below the Coulomb barrier. As a quantum-mechanical interaction between particles, the nuclear nonresonance reaction probability is proportional to a geometrical factor, which is inversely proportional to E — the energy in the center-of-mass reference frame of the colliding particles.

This is the reason for the following parametrization of the cross section:

$$\sigma_{ab} = \frac{1}{E}\, S_{ab}(E)\, e^{-2\pi \eta(E)}. \tag{6}$$

The function $S_{ab}(E)$, called the astrophysical S factor, incorporates all the nuclear physics effects (including effects of finite nuclear size, higher partial waves, anti-symmetrization, and atomic shielding). At low energies relevant for the solar fusion reactions and for many other astrophysics processes, the reaction cross sections are very small, typically of the order of 10^{-36}–10^{-33} cm^2 = 0.001–1 nb and with decreasing energy it becomes increasingly more difficult to measure them in the laboratory. Since the S factors are slowly varying, they can be more reliably extrapolated from the range of energies spanned by experimental data to the lower energies of astrophysical interest. Comprehensive compilations of the astrophysical S factors and relevant references can be found in [15–17].

Substituting the definition (6) into (5) yields

$$\langle \sigma_{ab} v \rangle = \frac{1}{\sqrt{\pi \mu}} \left(\frac{2}{kT} \right)^{3/2} \int_0^\infty S_{ab}(E)\, e^{-\chi(E)} dE, \quad \chi(E) = \sqrt{\frac{E_G}{E}} + \frac{E}{kT}.$$

Considering that the S factor is a smooth function, while the function χ has a sharp minimum (and thus $e^{-\chi}$ has a sharp maximum — Gamow peak), the integral can be evaluated by the saddle-point technique. The minimum of χ is given by the condition $d\chi/dE = 0$. Thence, the Gamow-peak energy (the root of the equation $d\chi/dE = 0$) is given by [1]

$$E_0 = E_G \left(\frac{kT}{2E_G} \right)^{2/3} \simeq 0.122 \left(A Z_a^2 Z_b^2 T_9^2 \right)^{1/3} \text{ MeV},$$

---

[1]Sometimes this quantity is also called Gamow energy and this may cause a confusion.

where $T_9 = T/(10^9 \text{ K})$. In the vicinity of the Gamow peak the function $\chi(E)$ can be fairly well approximated by the parabola:

$$\chi(E) \simeq \chi(E_0) + \frac{1}{2} \left[\frac{d^2\chi(E_0)}{dE_0^2} \right] (E - E_0)^2 = \tau + 4 \left(\frac{E - E_0}{\Delta} \right)^2,$$

where

$$\tau = \frac{3E_0}{kT} = 3 \left(\frac{E_G}{4kT} \right)^{1/3} \simeq 4.25 \left(\frac{AZ_a^2 Z_b^2}{T_9} \right)^{1/3}$$

and

$$\Delta = 4\sqrt{\frac{kTE_0}{3}} \simeq 0.237 \left(AZ_a^2 Z_b^2 T_9^5 \right)^{1/6} \text{ MeV}.$$

Clearly Δ defines the width of the Gamow window — the energy region where the reaction $a + b \to c + \ldots$ mainly operates[1]. Finally we obtain

$$\langle \sigma_{ab} v \rangle \simeq \sqrt{\frac{2}{\mu kT}} \frac{\Delta}{kT} S_{ab}(E_0) \, \mathrm{e}^{-\tau} \simeq$$

$$\simeq 1.3 \cdot 10^{-14} \left(\frac{Z_a Z_b}{A T_9^2} \right)^{1/3} S_{ab}(E_0) \, \mathrm{e}^{-\tau} \text{ cm}^3/(\text{s} \cdot \text{MeV} \cdot \text{b}). \tag{7}$$

At a given temperature, the factor $\mathrm{e}^{-\tau}$ in (7) is very sensitive to the charges of the interacting nuclei and less sensitive to their neutron content. The approximate formula (7) can be essentially improved by accounting for the next-order corrections to the saddle-point approximation and for the screening effect of the solar plasma electrons [18]. Then $S_{ab}(E_0)$ in (7) is replaced with $f_{ab} S_{ab}^{\text{eff}}$, where

$$S_{ab}^{\text{eff}} \simeq S_{ab}(E_0) + \frac{1}{\tau} \left[\frac{5}{12} S_{ab}(E_0) + \frac{5}{2} S_{ab}'(E_0) E_0 + S_{ab}''(E_0) E_0^2 \right] \simeq$$

$$\simeq S_{ab}(0) \left(1 + \frac{5}{12\tau} \right) + S_{ab}'(0) E_0 \left(1 + \frac{35}{12\tau} \right) + \frac{1}{2} S_{ab}''(0) E_0^2 \left(1 + \frac{89}{12\tau} \right)$$

and f_{ab} is the screening enhancement factor which allows for a partial shielding of the Coulomb potential of the nuclei, owing to the field of neighbouring electrons (see [16,17] for detail and further references). There are many other potentially significant physical effects neglected in (7), e.g., suppression of the reaction rates instead of enhancement [19], bound electron screening [20], non-Maxwellian tails of particle distributions (caused by plasma effects, relativistic and quantum corrections) [21], etc. Formally, many of them can be thought to be included into the factors f_{ab} or S_{ab}^{eff}, but usually they are just ignored in the standard solar model calculations.

In general a particle a can be affected by many nuclear reactions and decays, which either create or destroy it. So, the relative mass fraction (weight concentration) of particles a

$$X_a = \frac{m_a n_a}{\rho} \simeq \frac{m_H n_a A_a}{\rho} = \frac{n_a A_a}{N_A \rho}$$

---

[1]More precisely, Δ corresponds to the full width of the integrand at $1/e$ of its maximum, when approximated as a Gaussian. The full width of the Gamow window at half maximum is therefore given by $\Delta/\sqrt{\ln 2} \simeq 1.2\Delta$.

changes with time (here and below ρ is the density in units of g/cm^3). Then we have

$$\frac{\partial X_a}{\partial t} = \frac{m_a}{\rho} \left[\sum R_{b \to a + \ldots} + \sum R_{b+c \to a + \ldots} - \sum R_{a \to \ldots} - \sum R_{a+b' \to \ldots} \right], \qquad (8)$$

where «...» denote the sets of particles allowed by the conservation laws, and the summations extend over all relevant reactions and decays. Equation (8) can be corrected by adding the triple collision reactions and so on. The reaction rates in (8) are functions of the relative mass fractions: $R_{b \to a + \ldots} \propto n_b \propto X_b$, $R_{b+c \to a + \ldots} \propto n_b n_c \propto X_b X_c$, etc. Therefore, the full set of equations (8) constitute a network of first-order nonlinear differential equations. Solution of these coupled equations with the proper initial conditions and identity $\sum_a X_a = 1$ defines the chemical evolution of the Sun. The problem can be solved numerically, using, e.g., Runge–Kutta integration. However, the numerical methods are not always necessary, considering that many reactions quickly come to «equilibrium» and their rates can be evaluated analytically.

4. THE PP FUSION STEP BY STEP

4.1. The pp I Branch. The proton–proton chain begins by fusing two hydrogen nuclei:

$$p + p \to d + e^+ + \nu_e. \qquad (9)$$

The energy liberation, Q, in this reaction is 1.442 MeV, including in average ~ 0.265 MeV taking away by neutrinos ($E_\nu \lesssim 422$ keV). Using the results of the previous section, we can write the deuterium production rate (in units s^{-1}):

$$\frac{\partial X_d}{\partial t} \equiv \dot{X}_d = C_{11} \rho X_p^2 T_9^{-2/3} \exp\left(-3.38 T_9^{-1/3}\right), \quad C_{11} \approx 4.2 \cdot 10^{-15}. \qquad (10)$$

The magnitude of the dimensionless coefficient C_{11} is defined by the astrophysical S factor $S_{pp} \equiv S_{11} \simeq 4 \cdot 10^{-19}$ eV $\cdot$ b, and its calculation is well beyond the scope of this paper. It is however easy to understand why S_{pp} is so small.

A free proton cannot decay into a neutron because it has less mass, but a proton bound inside a nucleus may be in a higher energy state than the final neutron, and the inverse β decay (β^+ decay) can proceed. Therefore, the reaction (9) requires that two protons form a coupled system ^{2}He («diproton») while flashing past one another and, practically at the same instant, one of the bound protons must decay by emitting a positron and neutrino. The remaining proton and neutron are then left together forming a rather fragile deuteron (2.22 MeV binding energy). This sequence of events is very unlikely since the intermediate nucleus ^{2}He is highly unstable and much more frequently decays back to two protons [1].

The secondary positron created in the reaction (9) very quickly encounters a free electron in the surrounding plasma, the e^+ and e^- annihilate and their energy appears as two 511-keV γ quanta, but one time in (roughly) 10^{20}, the $e^+ e^-$ annihilation yields a $\nu \overline{\nu}$ pair instead.

---

[1] For this reason the cross section of the reaction (9) will probably never be measured in a laboratory experiment and we may rely only on the *ab initio* theory, which is, however, believed to be as accurate as $\pm 0.7\%$ around the Gamow peak [17].

The characteristic time of the reaction (9) (that is the mean life of a proton against destruction by this reaction) can be estimated as

$$t_{11} = \frac{n_p}{-\dot{n}_p} = \frac{n_p}{2\dot{n}_d},$$

where the factor of 2 in the denominator appears because each reaction destroys two protons. Substituting typical values $T = 1.3 \cdot 10^7$ K, $\rho = 100$ g/cm^3 and $X_p = 0.7$, we find that $t_{11} \approx 10^{10}$ y. So, the reaction is very rare. That is why the Sun is still burning after about $4.6 \cdot 10^9$ y of its life!

The deuterium produced in the first stage of the pp I branch can fuse with another free proton to form a light stable isotope of helium (helion):

$$p + d \rightarrow {}^3\text{He} + \gamma. \tag{11}$$
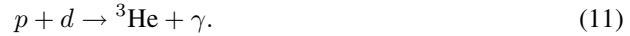
A photon must be emitted to avoid energy-momentum violation. Hence, the reaction goes via both strong and electromagnetic interactions. This reaction can be considered in a fashion similar to (9). The energy liberation here is much larger, $Q = 5.494$ MeV, and the production rate is

$$\dot{X}_{{}^3\text{He}} = C_{12}\rho X_p X_d T_9^{-2/3} \exp\left(-3.72 T_9^{-1/3}\right), \quad C_{12} \approx 3.98 \cdot 10^3. \tag{12}$$

Note that $C_{12}/C_{11} \approx 10^{18}$. Deuterium is burned up very rapidly, with the typical reaction time $t_{12} \approx 6$ s. Now α particles can be produced by fusing two ^{3}He nuclei:

$$^3\text{He} + {}^3\text{He} \rightarrow 2p + {}^4\text{He}. \tag{13}$$

This is the final stage of the branch and sometimes just this reaction is referred to as the pp I branch. The energy liberation is $Q = 12.859$ MeV and the ^{4}He production rate is given by

$$\dot{X}_{{}^4\text{He}} = C_{33}\rho X_{{}^3\text{He}}^2 T_9^{-2/3} \exp\left(-12.28 T_9^{-1/3}\right), \quad C_{33} \approx 1.3 \cdot 10^{10}. \tag{14}$$

The coefficient C_{33} is so huge because the reaction proceeds exclusively via the strong interaction. The characteristic time is $t_{33} \approx 10^6$ y.

A few concluding comments come in order.

For each conversion of four protons to ^{4}He, reactions (9) and (11) have to occur twice, while reaction (13) once. As we see, even at the solar core temperatures, the average lifetime of a proton against the pp fusion is $\sim 10^{10}$ y. It is this time scale that sets the «stellar clock» by determining how long the Sun will remain a stable main sequence object. In contrast, a deuterium nucleus will last only a few seconds before it hits into some proton. Therefore, deuterium cannot accrue and its steady concentration is given by $X_d = (t_{12}/t_{11})X_p \approx 10^{-17} X_p$. A helion will last hundreds thousands years before it hits another helion which has enough energy to overcome Coulomb's barrier.
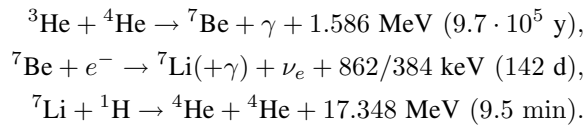
The deuterium is also produced in the extremely rare three-body reaction of electron capture (called pep)

$$p + p + e^- \rightarrow d + \nu_e \quad (E_\nu = 1.442 \text{ MeV}),$$

which yields an almost «monochromatic» neutrino. The neutrino energy spread is determined only by the small Doppler effect and almost negligible energy contributed to the recoil of the

deuterium nucleus. The characteristic time scale of the reaction is $\sim 10^{12}$ y, which is much larger than the age of Universe. So it is insignificant in the Sun as far as energy generation is concerned. Nevertheless, the *pep* fusion accounts for about 0.25% of the deuterons created in the *pp* chain. Enough *pep* fusions happen to produce a detectable number of the sharp-energy-line neutrinos, so the reaction must be accounted for by those interested in the solar neutrino problem.
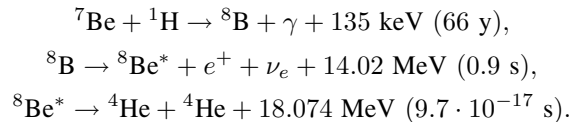
4.2. The *pp* II Branch. The ^{3}He does not always have to hit another ^{3}He nucleus. If ^{4}He is sufficiently abundant, ^{3}He can hit a ^{4}He forming stable ^{7}Be which can capture a free electron. The electron turns one of the beryllium protons into a neutron, changing the ^{7}Be into ^{7}Li and emitting a neutrino. The ^{7}Li will then quickly fuse with a free proton, resulting in unstable ^{8}Be which immediately falls apart into two stable ^{4}He nuclei. The branch is summarized in the following table:

$$^3\text{He} + {}^4\text{He} \rightarrow {}^7\text{Be} + \gamma + 1.586 \text{ MeV} \ (9.7 \cdot 10^5 \text{ y}),$$

$$^7\text{Be} + e^- \rightarrow {}^7\text{Li}(+\gamma) + \nu_e + 862/384 \text{ keV} \ (142 \text{ d}),$$

$$^7\text{Li} + {}^1\text{H} \rightarrow {}^4\text{He} + {}^4\text{He} + 17.348 \text{ MeV} \ (9.5 \text{ min}).$$

The ^{4}He nucleus acts here as a catalyst to the conversion of ^{3}He and proton into ^{4}He. Only about 14% of ^{3}He goes out this way avoiding the *pp* I branch. Almost all ($\sim 99.89\%$) ^{7}Be nuclei go the lithium route. The main part ($\sim 89.7\%$) of ^{7}Li nuclei is created in the ground state and thus $E_\nu \approx 862$ keV. The rest lithium is in an excited state and the corresponding neutrino energy is only 384 keV. The largest contribution to the uncertainty in the prediction of the beryllium neutrino flux is caused by the experimental uncertainty in the low-energy rate of the ^{3}He + ^{4}He reaction. The fusion with ^{4}He is less likely, because there is more ^{3}He around deep inside the Sun's core.

In heavier stars, where the temperatures exceed $\sim 2.4 \cdot 10^7$ K, the *pp* II branch can compete with the *pp* I branch for energy production. This is because at higher temperatures ^{3}He gets used up faster, driving down its abundance compared to ^{4}He. On the contrary, in low-mass stars the internal temperature is not high enough to finish the *pp* cycle. They give rise to the first stage of the *pp* fusion up to ^{3}He, but are unable to force the fusion of ^{3}He with another helium isotope. This fact is confirmed by the observation that the low-mass stars are often anomalously rich in ^{3}He compared to ^{4}He.

4.3. The *pp* III Branch. The ^{7}Be has two ways to go — it can either absorb an electron, as in the *pp* II branch (99.89%), or absorb a proton (0.11%). Absorbing a proton raises the nucleus from beryllium to boron, and the ^{7}Be becomes ^{8}B. The latter nucleus is unstable and takes less than a second, fairly independent of temperature, to spit out a positron and a neutrino to become beryllium again, only this time it is ^{8}Be, which falls apart into two ^{4}He nuclei, thus completing the chain:

$$^7\text{Be} + {}^1\text{H} \rightarrow {}^8\text{B} + \gamma + 135 \text{ keV} \ (66 \text{ y}),$$

$$^8\text{B} \rightarrow {}^8\text{Be}^* + e^+ + \nu_e + 14.02 \text{ MeV} \ (0.9 \text{ s}),$$

$$^8\text{Be}^* \rightarrow {}^4\text{He} + {}^4\text{He} + 18.074 \text{ MeV} \ (9.7 \cdot 10^{-17} \text{ s}).$$

Only $\sim 0.11\%$ of ^{7}Be goes this route. The so-called boron neutrinos produced in this chain have a rather high mean energy, $\langle E_\nu \rangle \simeq 6.74$ MeV, and their energy spectrum spreads up to

14.02 MeV. This makes it possible to detect the boron neutrinos, despite of their relatively small flux. The boron neutrino flux Φ_ν^{B} is highly responsive to the quality of the solar modelling; in particular, it is extremely sensitive to the *central* temperature T_c, as it varies as T_c^{18}. For comparison, the central temperature dependence of the pp and beryllium neutrino fluxes are $\Phi_\nu^{pp} \propto T_c^{-1.2}$ and $\Phi_\nu^{\mathrm{Be}} \propto T_c^{8}$, respectively. These dependences correspond to the neutrino fluxes from each source integrated over the relevant region of emission. Just for the central conditions in the Sun, the T_c dependences for the three major neutrino fluxes can be expressed in the following way: $\Phi_\nu^{pp} \propto T_c^{4}$, $\Phi_\nu^{\mathrm{Be}} \propto T_c^{11.5}$, $\Phi_\nu^{\mathrm{B}} \propto T_c^{24.5}$. Another very significant source of ambiguity in the prediction of the boron neutrino flux is caused by the uncertainty in the laboratory measurements of the $^7\mathrm{Be}(p,\gamma)^8\mathrm{B}$ S factor S_{17}. The present-day resulting uncertainty of S_{17} in the solar Gamow window is $\pm 7.5\%$ [17].

4.4. The pp IV Branch (hep Reaction). This branch comprises the only fusion process

$$^3\mathrm{He} + {}^1\mathrm{H} \rightarrow {}^4\mathrm{Li} \rightarrow {}^4\mathrm{He} + e^+ + \nu_e + 19.795 \text{ MeV.}$$
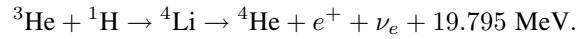
The low-energy cross section of this «hep reaction» is very uncertain ($\pm 30\%$ according to [17]). This ambiguity is not important from the point of view of the solar energy production, since the relative probability of the pp IV branch is estimated to be as small as $(2-3) \cdot 10^{-5}\%$. However, the hep reaction produces the highest-energy solar neutrinos [1] ($\langle E_\nu \rangle \simeq 9.625$ MeV, $E_\nu \lesssim 18.778$ MeV), which can at some level influence the electron energy spectrum produced by the solar neutrino interactions and measured in the high-threshold detectors like Super-Kamiokande and SNO.

4.5. The Full pp Chain. The diagram in Fig. 1 summarizes the full pp chain. The neutrinos export 3%, 4%, and 28% of the energy in, respectively, pp I, pp II, and pp III. The pp II and pp III chains have an output of two $^4\mathrm{He}$ nuclei, but require an input of one $^4\mathrm{He}$. The net
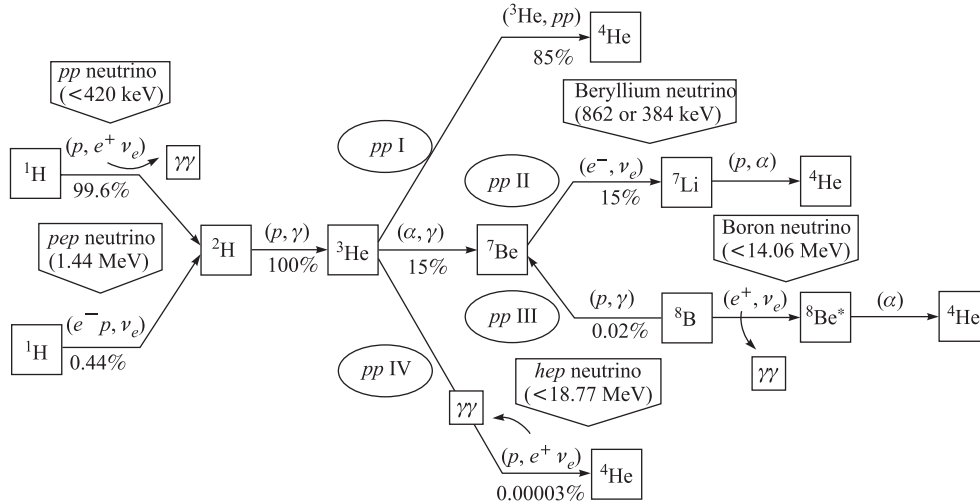

Fig. 1. The full pp chain responsible for production of about 98.4% of the solar energy

---

[1]The maximum neutrino energy is equal to the maximum energy of the $^4\mathrm{Li}$ β decay.

effect is the fusion of one ^{4}He nucleus per reaction sequence and hence one of the ^{4}He nuclei acts only as a catalyst which allows ^{7}Be production. In any hydrogen-burning star containing significant ^{4}He abundance, all the four pp chains are active simultaneously. The Sun is a perfect example of such a star.

4.6. Is the pp Chain Complete? One can invent many other reaction embedded into the pp chain, some of which will produce neutrinos. But careful analysis shows that the corresponding contributions to both energy production and neutrino production are very small. Let us consider several illustrations (see [22, 23] for other examples).

Tritium Neutrinos and Antineutrinos. The neutrinos can be produced in the rare endothermic electron capture reaction [24]

$$^3\text{He} + e^- \rightarrow {}^3\text{H} + \nu_e \quad (E_e \gtrsim 18.6 \text{ keV}, \ t \approx 1.4 \cdot 10^{11} \text{ y}). \tag{15}$$

The chain is completed with the fusion reaction $^3\text{H} + p \rightarrow {}^4\text{He} + \gamma$ ($E_\gamma \approx 19.8$ MeV). However, the energies of the tritium neutrinos are within the range from 2.5 to 3 keV and there is no good idea about how to detect such low-energy neutrinos. Moreover, the flux of these neutrinos at the Earth is only $8.1 \cdot 10^4$ cm$^{-2} \cdot$ s^{-1}.

The capture (15) can be followed by the tritium β^- decay with production of *antineutrinos* with energies up to about 18.6 keV. Their flux at the Earth is estimated in [24] to be about 10^3 cm$^{-2} \cdot$ y^{-1}. Alas! Both the energy and the flux are very small. This does not allow detecting the tritium antineutrinos in the foreseeable-future experiments.

The pp V Branch (heep Reaction). It was mentioned above that neutrinos with maximum energy ($E_\nu^{\max} \approx 18.8$ MeV) are produced in the hep reaction. But, in fact, the most energetic solar neutrinos are produced in the so-called $heep$ reaction [23]

$$^3\text{He} + e^- + p \rightarrow {}^4\text{He} + \nu_e \quad (E_\nu \approx 19.8 \text{ MeV}). \tag{16}$$

Unfortunately, the estimated flux is only $2.5 \cdot 10^{-4}$ cm$^{-2} \cdot$ s^{-1} [24], which is about four orders of magnitude less than the flux of the hep neutrinos near the end of their spectrum.

Electron Capture on ^{8}B. Very high-energy neutrinos are also produced in the e-capture reaction [22, 25]

$$^8\text{B} + e^- \rightarrow {}^8\text{Be}^* + \nu_e, \quad {}^8\text{Be}^* \rightarrow {}^4\text{He} + {}^4\text{He}.$$
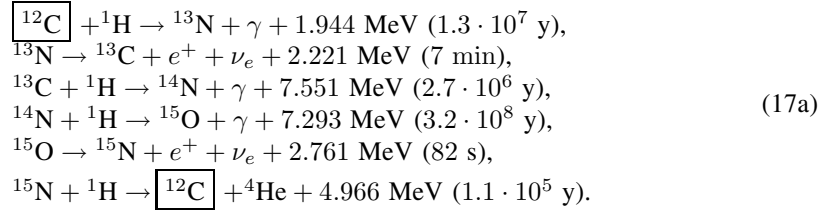
The neutrino energy spectrum from this reaction peaks near 15.5 MeV and has a full width at half maximum of about 1.4 MeV. The neutrino flux is estimated to be (1.3 ± 0.2) cm$^{-2} \cdot$ s^{-1} [25]. Though it is almost four orders of magnitude larger than that of the $heep$ neutrinos, it is still too small to be detected in the current experiments.
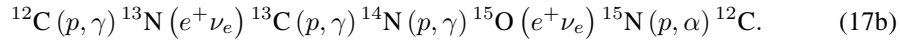
5. THE CNO CYCLE

The matter that formed the Sun had already been cycled through one or more generations of stars and, as a result, it is contaminated with all the stable elements of the periodic table (see Subsec. 6.3). The presence of these ashes of deceased stars in the solar core opens possibility for the fusion reaction sequences, which require certain heavy elements as catalytic agents. The next in importance (after the pp chain) is the CNO polycycle responsible for as much as 1.6% of the energy production in the Sun.

5.1. Cycle I (CN). The main CNO reaction sequence («cycle I» or «CN cycle»)[1] is
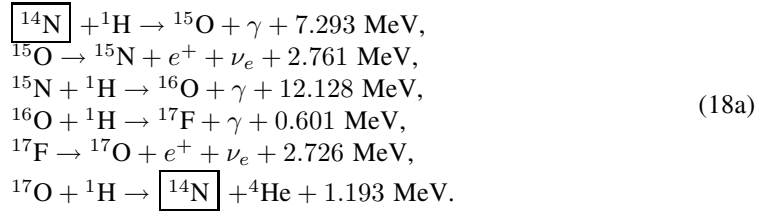
$$
\begin{aligned}
\boxed{^{12}\text{C}} + {}^1\text{H} &\to {}^{13}\text{N} + \gamma + 1.944 \text{ MeV } (1.3 \cdot 10^7 \text{ y}), \\
{}^{13}\text{N} &\to {}^{13}\text{C} + e^+ + \nu_e + 2.221 \text{ MeV } (7 \text{ min}), \\
{}^{13}\text{C} + {}^1\text{H} &\to {}^{14}\text{N} + \gamma + 7.551 \text{ MeV } (2.7 \cdot 10^6 \text{ y}), \\
{}^{14}\text{N} + {}^1\text{H} &\to {}^{15}\text{O} + \gamma + 7.293 \text{ MeV } (3.2 \cdot 10^8 \text{ y}), \\
{}^{15}\text{O} &\to {}^{15}\text{N} + e^+ + \nu_e + 2.761 \text{ MeV } (82 \text{ s}), \\
{}^{15}\text{N} + {}^1\text{H} &\to \boxed{^{12}\text{C}} + {}^4\text{He} + 4.966 \text{ MeV } (1.1 \cdot 10^5 \text{ y}).
\end{aligned}
\tag{17a}
$$

This sequence is clearly a cycle since the last reaction restores the initial ^{12}C. The cycle (17a) becomes even more apparent being rewritten in the compact astrophysical notation:

$$
{}^{12}\text{C}\,(p,\gamma)\,{}^{13}\text{N}\,\left(e^+\nu_e\right)\,{}^{13}\text{C}\,(p,\gamma)\,{}^{14}\text{N}\,(p,\gamma)\,{}^{15}\text{O}\,\left(e^+\nu_e\right)\,{}^{15}\text{N}\,(p,\alpha)\,{}^{12}\text{C}.
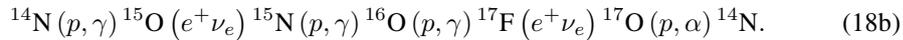\tag{17b}
$$

The cycle uses carbon, nitrogen and oxygen isotopes as catalysts to suck up four protons and build a ^{4}He nucleus out of them. The relative abundances of C, N, and O do not change. The cycle does not start until the *pp* fusion has begun, and provides the energy necessary to allow a low level of proton fusions onto the heavier nuclei. The timescale of the CN cycle is determined by the slowest reaction (^{14}N + ^{1}H), while the approach to equilibrium is determined by the second slowest reaction (^{12}C + ^{1}H).

5.2. Cycle II (ON). The second minor branch («cycle II» or «ON cycle») is a similar type of cycle which joins onto the first one. Starting with ^{14}N, the process steps through two of the last three reactions (17) until ^{15}N is produced. It then proceeds to convert ^{15}N back into ^{14}N, with the production of ^{17}F occurring in one of the steps:

$$
\begin{aligned}
\boxed{^{14}\text{N}} + {}^1\text{H} &\to {}^{15}\text{O} + \gamma + 7.293 \text{ MeV}, \\
{}^{15}\text{O} &\to {}^{15}\text{N} + e^+ + \nu_e + 2.761 \text{ MeV}, \\
{}^{15}\text{N} + {}^1\text{H} &\to {}^{16}\text{O} + \gamma + 12.128 \text{ MeV}, \\
{}^{16}\text{O} + {}^1\text{H} &\to {}^{17}\text{F} + \gamma + 0.601 \text{ MeV}, \\
{}^{17}\text{F} &\to {}^{17}\text{O} + e^+ + \nu_e + 2.726 \text{ MeV}, \\
{}^{17}\text{O} + {}^1\text{H} &\to \boxed{^{14}\text{N}} + {}^4\text{He} + 1.193 \text{ MeV}.
\end{aligned}
\tag{18a}
$$

The same can be written as

$$
{}^{14}\text{N}\,(p,\gamma)\,{}^{15}\text{O}\,\left(e^+\nu_e\right)\,{}^{15}\text{N}\,(p,\gamma)\,{}^{16}\text{O}\,(p,\gamma)\,{}^{17}\text{F}\,\left(e^+\nu_e\right)\,{}^{17}\text{O}\,(p,\alpha)\,{}^{14}\text{N}.
\tag{18b}
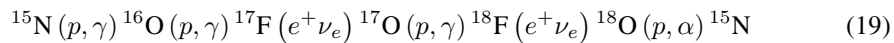$$

The third reaction of the cycle has a probability of about $4 \cdot 10^{-4}$ relative to the last reaction of the cycle (17). As a result, the ON cycle is about 25 times less frequent than the CN cycle.

5.3. The Full CNO Polycycle. The diagram in Fig. 2 shows the full CNO bicycle. The fractions of the nuclear energy loss from the core through neutrino emission in the first and second branches of the CNO process are 6 and 4%, respectively. In fact, there are two extra CNO chains:

$$
{}^{15}\text{N}\,(p,\gamma)\,{}^{16}\text{O}\,(p,\gamma)\,{}^{17}\text{F}\,\left(e^+\nu_e\right)\,{}^{17}\text{O}\,(p,\gamma)\,{}^{18}\text{F}\,\left(e^+\nu_e\right)\,{}^{18}\text{O}\,(p,\alpha)\,{}^{15}\text{N}
\tag{19}
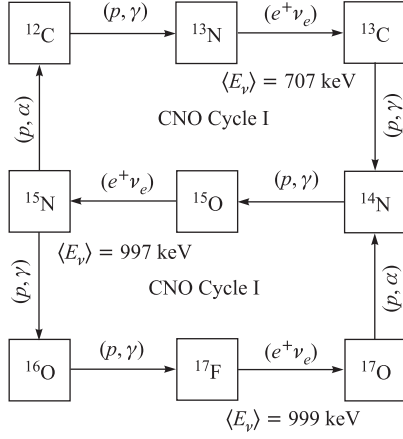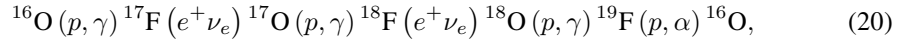$$

---

[1] Other names are «simple CN cycle», «carbon(ic) cycle», and «Bethe cycle».

Fig. 2. The full CNO bicycle responsible for production of about 1.5–1.6% of the solar energy. Cycle I dominates
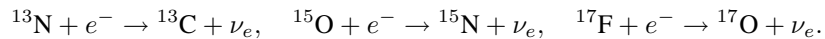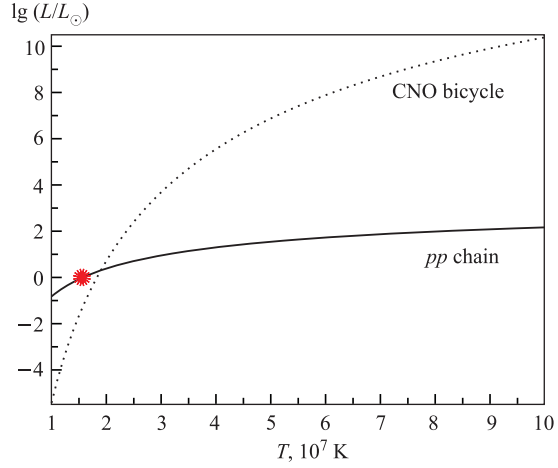

Fig. 3. The stellar energy production vs. temperature for the pp chain and CNO bicycle, showing the dominance of the former at solar temperatures. Solar metallicity has been assumed

and

$$^{16}\mathrm{O}\,(p,\gamma)\,^{17}\mathrm{F}\left(e^{+}\nu_{e}\right)\,^{17}\mathrm{O}\,(p,\gamma)\,^{18}\mathrm{F}\left(e^{+}\nu_{e}\right)\,^{18}\mathrm{O}\,(p,\gamma)\,^{19}\mathrm{F}\,(p,\alpha)\,^{16}\mathrm{O}, \tag{20}$$

and a few accessory reaction chains embedded into the main polycycle [16]:

$$^{13}\mathrm{N}\,(p,\gamma)\,^{14}\mathrm{O}\left(e^{+}\nu_{e}\right)\,^{14}\mathrm{N},\,^{17}\mathrm{F}\,(p,\gamma)\,^{18}\mathrm{Ne}\left(e^{+}\nu_{e}\right)\,^{18}\mathrm{F}\,(p,\alpha)\,^{15}\mathrm{O},\,^{19}\mathrm{F}\,(p,\gamma)\,^{20}\mathrm{Ne}.$$

The chain (19) («CNO cycle III» or «ON II cycle») is essential for the hydrogen burning in massive stars but almost negligible in the Sun. The cycle (20) is very slow and its role for both energy production and neutrino production in stars is insignificant.

The CNO cycle lacks significance at the low temperatures. For abundances characteristic of the Sun, the CNO becomes important for core temperatures of roughly $1.5 \cdot 10^7$ K (1.3 keV), and it will provide virtually all of the hydrogen-to-helium conversion in the later stages of the solar evolution when the temperature will exceed $\approx 2.5 \cdot 10^7$ K (2.2 keV), as is seen in Fig. 3 (taken from [17]). The sprocket symbol in Fig. 3 denotes the present-day conditions in the Sun's center, $T = 1.57 \cdot 10^7$ K, showing that the Sun is now powered mainly by the pp chain.

5.4. CNO Electron Capture. As was shown above, the CNO sources of neutrinos are the β^+ decays of ^{13}N, ^{15}O, and ^{17}F. An additional (minor) contribution to the CNO neutrino flux, usually not included into the solar models, is electron capture (EC) on those isotopes [23,26]. The relevant reactions are

$$^{13}\mathrm{N} + e^- \rightarrow\, ^{13}\mathrm{C} + \nu_e, \quad ^{15}\mathrm{O} + e^- \rightarrow\, ^{15}\mathrm{N} + \nu_e, \quad ^{17}\mathrm{F} + e^- \rightarrow\, ^{17}\mathrm{O} + \nu_e.$$

At solar temperatures and densities one must take into account the contribution from both bound (mainly K-shell) and continuum electrons. The flux of the CNO EC neutrinos is of the same order as the boron neutrino flux, though at lower neutrino energies. So the rate of these neutrinos on current detectors is expected to be very small but not fully negligible [26].

6. SOLAR NEUTRINO FLUX AND SPECTRUM

6.1. Neutrino Flux–Luminosity Relation. The Sun is approximately in a steady state with the energy production rate that equals its luminosity, hence the total solar neutrino flux at the Earth is [27]

$$\Phi_\nu \approx \frac{2S_\odot}{Q - 2\langle E_\nu \rangle},$$

where $S_\odot = L_\odot/4\pi d_\odot^2 \simeq 1.366$ kW/m^2 is the satellite measured solar constant[1] which yields the solar luminosity $L_\odot = 4\pi d_\odot^2 \approx 3.846 \cdot 10^{33}$ erg/s for $d_\odot = 1$ AU $\approx 1.496 \cdot 10^{13}$ cm; $\langle E_\nu \rangle$ is the mean energy of the solar neutrinos given by

$$\langle E_\nu \rangle = \frac{1}{\Phi_\nu} \sum_i E_\nu^{(i)} \Phi_\nu^{(i)},$$

where the summation extends over all reactions which produce neutrinos, $E_\nu^{(i)}$ and $\Phi_\nu^{(i)}$ are, respectively, the mean energy and neutrino flux from the ith reaction. The value of $\langle E_\nu \rangle$ can be well approximated by the mean energy of the pp neutrinos $\langle E_\nu^{(pp)} \rangle \approx 0.265$ MeV, which dominate the solar neutrino flux. Since $\langle E_\nu^{(pp)} \rangle \ll Q$, the inaccuracy of this approximation does not essentially affect the estimation of Φ_ν. Finally we obtain

$$\Phi_\nu \approx 6.54 \cdot 10^{10} \text{ cm}^{-2} \cdot \text{s}^{-1}.$$

This is a huge value and it is almost model-independent. Calculation of the neutrino energy spectrum is a much more difficult, but necessary, task, which requires lots of assumptions.

6.2. The Standard Solar Models. The present-day Sun is a G2-type main-sequence star. Solar models evolve the Sun over the past 4.56 Gy of the main sequence burning to the present age, thereby predicting the present-day temperature and composition profiles, the relative strengths of competing nuclear reaction sequences, and the neutrino fluxes originating from those sequences. The standard solar models (SSM) share several basic assumptions:

• The Sun is a spherically symmetric object evolving in hydrostatic equilibrium which implies a local balance between pressure and gravity.

• The thermonuclear reactions are the only source of energy production inside the Sun. They do not change the abundances of heavy elements but transmute hydrogen to helium and produce a smooth variation of the remaining physical parameters.

• Energy is diffused by radiative, convective, and neutrino transports. The solar envelope is convective, while the core region where the thermonuclear reactions take place is dominated by radiative transport. The opacity of the solar medium sensitively depends on the chemical composition, particularly, on the heavy-element abundances.

• The Sun was initially highly convective and therefore uniform in composition, when it first entered the main sequence.

• The mass remains constant throughout the evolution.

---

[1]In fact, this «constant», defined as the power per unit area received at the average Sun–Earth distance of one Astronomic Unit (AU), varies within $\pm 0.1\%$ during an 11-year solar cycle.

Within the framework of these assumptions, the geometry, hydrostatic equilibrium, energy balance, and its transport are described by the four first-order differential equations of stellar structure (see, e.g., [28] and [29] for more details and further references),

$$\text{Continuity equation:} \quad \frac{dM}{dR} = 4\pi R^2 \rho,$$

$$\text{Hydrostatic equation:} \quad \frac{dP}{dR} = -\frac{GM\rho}{R^2},$$

$$\text{Energy equation:} \quad \frac{dL}{dR} = 4\pi R^2 \left[\epsilon\rho - \rho\frac{d}{dt}\left(\frac{u}{\rho}\right) + \frac{P}{\rho}\frac{d\rho}{dt} \right],$$

$$\text{Energy transfer equation:} \quad \frac{dT}{dR} = \nabla\frac{T}{P}\frac{dP}{dr}.$$

Here $R = |\mathbf{R}|$ is the distance to the center and t is the time (all variables involved into the above equations are functions of these two); G is the gravitational constant, P is the pressure [1], M is the mass enclosed in the sphere of radius R («shell mass»), ρ is the density, T is the temperature, L is the flow of energy per unit time through the sphere of radius R, ϵ is the rate of nuclear energy generation per unit mass and time, and u is the internal energy per unit volume. The temperature gradient $\nabla = d\ln T/d\ln P$ is determined by the mode of the energy transport.

Apart from the basic equations, one has to specify the auxiliary ones: $\rho = \rho(P, T, \{X_a\})$ (equation of state), $\kappa = \kappa(P, T, \{X_a\})$ (equation for opacity), and $\epsilon = \epsilon(P, T, \{X_a\})$ (equation for nuclear reaction rate); these link the thermal quantities and the chemical abundances X_a. The opacity κ (defined so that $1/(\kappa R)$ is the mean free path of a photon) enters the stellar structure equations through the temperature gradient $\nabla = \nabla_{\text{rad}} + \nabla_{\text{cond}} + \nabla_{\text{conv}}$, in which the terms denote, respectively, the radiative, conductive, and convective contributions. The radiative contribution, calculated under the assumption of local thermodynamic equilibrium, is given by

$$\nabla_{\text{rad}} = \frac{3}{16\pi a\tilde{c}G}\frac{\kappa P}{T^4}\frac{L}{M},$$

where $\tilde{c}$ is the speed of light, a is the radiation density constant. The conductive gradient is due to the electron plasma thermal motion and the convective gradient is acting only in the convective region, $R \gtrsim 0.7R_\odot$. In the regions where ∇_{rad} exceeds the adiabatic gradient $(\partial\ln/\partial\ln P)_s$, the partial derivative being taken at constant specific entropy s, the layer becomes unstable to convection. In that case, energy transport is predominantly by convective motion; the detailed description of convection is highly uncertain [29].

The main source of uncertainty for the opacity is the content of heavy elements in the solar core, which is out of experimental control. The SSM calculations assume that the surface abundances of the elements with $A > 5$ («metals» in astronomical slang) were undisturbed by the subsequent evolution and thus provide a record of the initial solar metallicity. This assumption is not quite correct. In fact, the present-day chemical composition of the photosphere must be slightly different from that of the protosolar gas cloud, owing to the combined

---

[1]In general, P is the sum of the gas, radiation and magnetic field $\mathbf{B}$ pressures, $P = P_{\text{gas}} + P_{\text{rad}} + \mathbf{B}^2/8\pi$, but the last contribution is normally neglected.

effects of thermal diffusion, gravitational settling, and radiative acceleration over the past 4.56 Gy. Additional, comparatively small changes are due to decay of radioactive isotopes that contribute to the overall atomic abundance of an element. However, all these effects can be taken into account as corrections or included into the initial conditions. The remaining unknown parameter is the initial mass fraction ratio ^{4}He/H. The helium content in the core cannot be directly measured, and thus it must be adjusted until the model reproduces the today's luminosity. The resulting value of ^{4}He/H in modern SSMs is typically 0.27 ± 0.01, which can be compared to the Big-Bang value of 0.23 ± 0.01. The present-day photospheric abundance is, of course, different from this value, owing to diffusion of helium over the lifetime of the Sun. The resulting ^{4}He abundance near the surface (typically 0.247) is in surprisingly good agreement with the value determined from helioseismology (0.242).

In addition to the listed physical approximations, any SSM depends on at least 19 parameters that must be supplied with their assigned uncertainties. The iterative solution of the basic equations with proper boundary conditions is starting from a zero-age main sequence object, and the output data are constrained to reproduce today's solar radius, mass, and luminosity.

We have to recognize that the standard solar models are based on many simplifications. Of these, one (but not the only one) of the most «fragile» is that the Sun is assumed to be a spherical star in hydrostatic equilibrium. We know, however, that the Sun slowly rotates around its axis in about 27 days. This causes a flattening of the solar surface which breaks the spherical symmetry, resulting in a reduction of the local gravity in the equatorial region, mixing of the solar atmosphere, and many other effects. Moreover, since the Sun is not a solid body, the rotation is not uniform. The outer layers exhibit differential rotation, which extends considerably down into the solar interior. These bulk motions affect the thermal stratification leading to significant mixing of chemical elements. In particular, fragile elements can be transferred to higher temperature layers where they are more rapidly destroyed. Traditional SSMs neglect all these details.
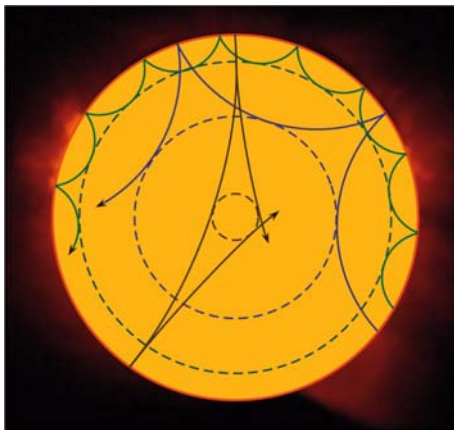
6.3. Helioseismology in Short. The solar surface vibrates like a huge drum. This phenomenon was discovered by Leighton, Noyes, and Simon [30] from systematic visual study of sets of «Doppler plates» obtained at the 13-foot spectroheliograph of the Mount Wilson Observatory during 1960 and 1961. Initially these «five-minute» oscillations were thought to be a manifestation of convective motions, but later it was understood that the observed motions are the superpositions of many global resonant modes of oscillations of the Sun (see, e.g., [29,31,32] for reviews and references). Solar oscillations consist of a reach spectrum of internal acoustic and gravity waves, stochastically excited by turbulent convection. Figure 4 schematically shows the propagation of sound rays in a cross section of the solar

Fig. 4. Propagation of sound rays in a cross section of the solar interior

interior. The ray paths are bent by the increase in sound speed with depth until they reach the inner turning point (indicated in the figure by the dashed circles), where they undergo total internal refraction. Near the surface the waves are reflected by the rapid decrease in density.

The raw data of helioseismology consist of measurements of the photospheric Doppler velocity or, in some cases, intensity in a particular wavelength band, taken at a cadence of about 1 min and collected with as little interruption as possible over periods of months or years [32]. An overview of the observation techniques can be found in [33].

Figure 5 (taken from [32]) shows a typical single Doppler velocity image of the Sun from one GONG (Global Oscillation Network Group) instrument. The shading across the first image comes from the solar rotation. After removing the rotation, the mottling associated primarily with the solar oscillations becomes apparent. The measurements of this kind can be either imaged or digitalized. The astronomers have learned how to use this information for studying the thermodynamic properties of the solar inside. Careful helioseismic studies contributed to the improvement of the determination accuracy of the radial distribution of sound speed in the Sun, differential rotation and so on.
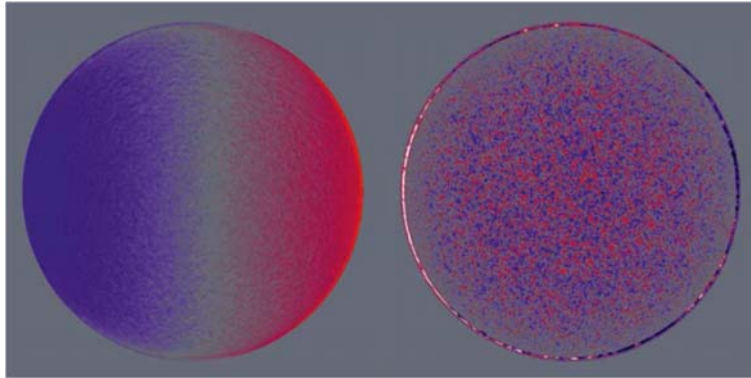

Fig. 5. A typical single Doppler velocity image of the Sun (left) and the difference between that image and the one taken a minute earlier (right) with the colors corresponding to motion away from and towards the observer

The adiabatic sound speed is a function of temperature and mean molecular weight. The gradient of the temperature, and hence of the sound speed, is related to the mechanism by which the heat is transported from the center to the surface. Both temperature and sound speed are influenced by the opacity of the solar matter to radiation, and the latter is influenced by the chemical composition of the Sun. The seismically determined sound speed is known today with a precision of the order of 0.001% for $R \gtrsim 0.4R_\odot$, allowing one to test and correct the theoretical estimates of the opacity and to cross-check the inputs for the solar composition. In the regions of the Sun where the neutrinos are generated, the resulting precision is degraded. Moreover, due to variation of the mean molecular weight with time, the sound speed slowly changes and has been modified by about 10% in the core during the life of the Sun [34]. Nevertheless, helioseismic analyses allow one to extract the squared sound speed in the core with an accuracy on the level of 0.01%. This provides a very useful benchmark for the solar models and helps to answer several questions (mixing in the solar core, influence of dynamic effects on the nuclear reaction rates, etc.) critical for determining the correct neutrino fluxes [35].

6.4. Chemical Composition of the Sun. As was explained above, the elemental abundances in the Sun is one of the key ingredients of any SSM. The chemical elements involved into the pp or CNO reactions directly affect the reaction rates and thus the solar neutrino fluxes.

The heavy elements as a whole are important as they govern radiative opacities, which in turn affect the density distribution in the outer convection zone and energy transport by the radiative transfer.

The elements up to and beyond ^{56}Fe are discovered in the solar atmosphere and in the pristine meteorites like CI-chondrites and ureilites (assumed to have the same composition as the Sun, excluding volatile elements) [36–44]. Some twenty years ago astrophysicists believed they knew the solar composition on the level sufficient for an accurate modeling of its evolution and inner structure. However, new analyses of absorption lines in the solar spectrum essentially downward the photospheric abundances of metals, compared to the previously used values. This is in particular true for the most abundant elements C, N, O, and Ne, which participate in the CNO polycycle.

The trend is illustrated in Fig. 6, which shows the mass fractions of hydrogen, helium, and metals (conventionally abbreviated as, respectively, $X = X_{\mathrm{H}}$, $Y = X_{\mathrm{He}}$, and $Z = 1 - X - Y$) as well as the metals-to-hydrogen ratio (Z/X). The data are taken from the comprehensive compilations [36] (AG89), [37] (GN93), [38] (GS98), [39] (L03), [40] (AGS05), [41] (AGSS09), and [43,44] (L10) and plotted as a function of year of publication. The figure shows the mass fractions for both the present-day photosphere and protosolar values, necessary as inputs of the solar models. Most of the differences seen in Fig. 6 are due to essential changes in modeling the solar atmosphere, upgrade of atomic and molecular data and better solar observations. The new solar chemical composition is supported by a high degree of internal consistency between available abundance indicators, and by agreement with values obtained in the Solar Neighborhood and from the most pristine meteorites. But, the SSM predictions based on the old GS98 metallicity were in fantastically good agreement (within 0.1 to 0.3% for most sophisticated SSM calculations) with the sound speed profiles precisely measured by helioseismic methods. The AGS05 result completely destroyed this agreement. The relative sound speed discrepancy for the AGS05-based solar models reaches
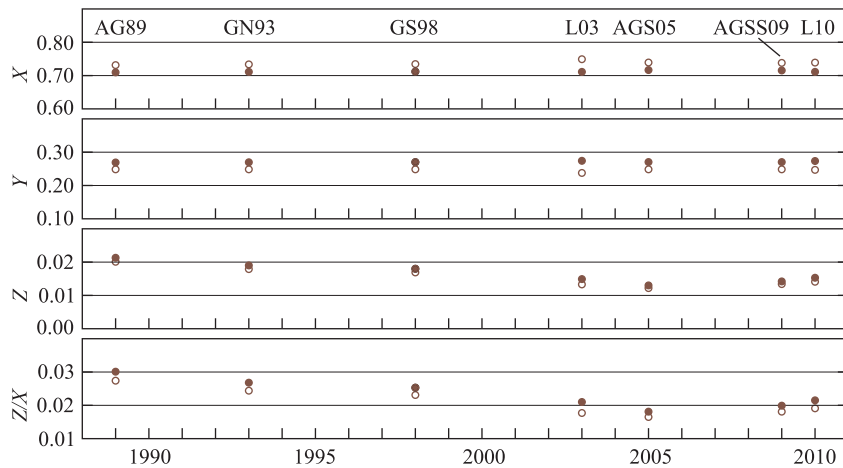

Fig. 6. Present-day photospheric (open circles) and protosolar (filled circles) mass fractions X, Y, Z and ratio Z/X taken from compilations [36–41,43,44]. Horizontal axis indicates the publication years. See text for the abbreviations in the top panel
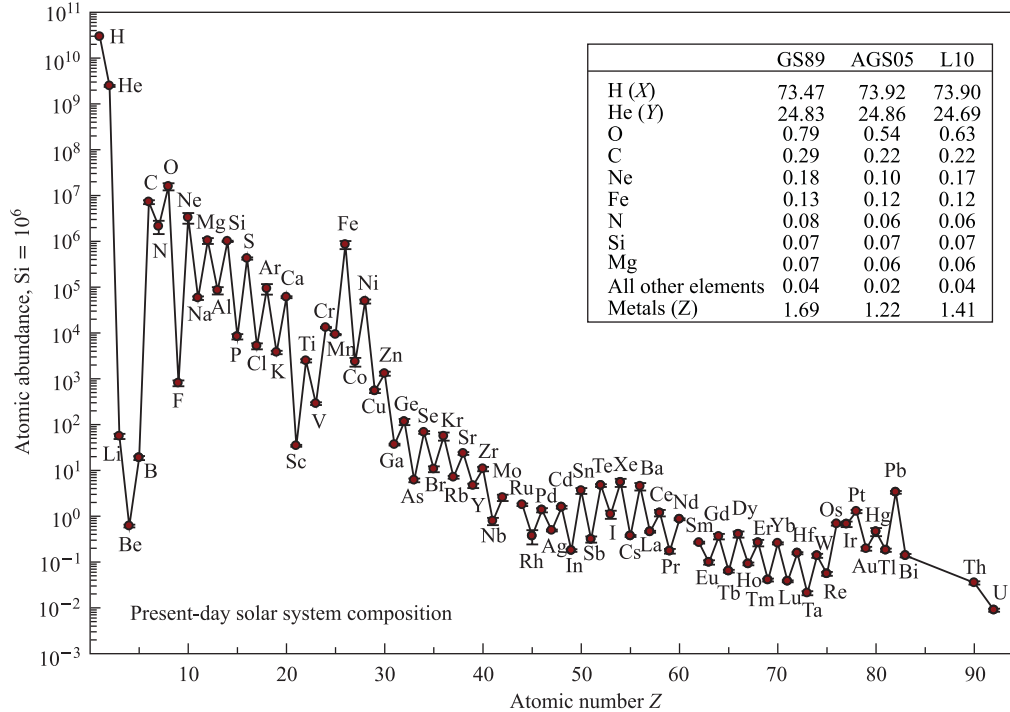
	GS89	AGS05	L10
H (X)	73.47	73.92	73.90
He (Y)	24.83	24.86	24.69
O	0.79	0.54	0.63
C	0.29	0.22	0.22
Ne	0.18	0.10	0.17
Fe	0.13	0.12	0.12
N	0.08	0.06	0.06
Si	0.07	0.07	0.07
Mg	0.07	0.06	0.06
All other elements	0.04	0.02	0.04
Metals (Z)	1.69	1.22	1.41

Fig. 7. Present-day solar system elemental abundances as function of atomic number normalized to 10^6 Si atoms [43]. The insert shows the present-day solar composition (mass %) according to [38] (GS98), [40] (AGS05), and [43] (L10)

about 1.2% immediately below the bottom of the convection zone. To date, there has been no fully convincing solution put forward. In the most up-to-date analyses L10 and AGSS09, the discordance has been alleviated somewhat relative to the AGS05 model, but it nevertheless remains a significant discrepancy in urgent need of resolution.

One of the modern versions of the present-day elemental abundance curve in the solar system is shown in Fig. 7, taken from the compilation [43]. The data presented in Fig. 7 are almost similar to those recommended in [41], but differ in details. The data of [43] are based on CI-chondrites, photospheric data, and theoretical calculations. In cases where solar and meteorite data have comparable accuracy for a given element, the recommended abundance is the average of these values. For other elements, meteoritic data seem more reliable. The general trend of the abundance curve is towards ever decreasing abundances as the atomic number increases. The distinct up-down zig-zag pattern is because the elements with *odd* numbers of nucleons (e.g., nitrogen, sodium, fluorine) are less stable, resulting in one unpaired (odd) proton or neutron. The huge drop in abundance for the Li–Be–B triplet results from two factors: (i) at the Big Bang, nuclear processes that could fuse the proper H or He isotopes into Li and/or the other two were statistically very rare and hence inefficient, and (ii) some of the Li–Be–B nuclei that were formed and survived were destroyed later on by reactions in stars. A very detailed plot and the tabulated data for the nuclide abundance distribution at the solar system formation time can be found in [43, 44].

6.5. Neutrino Energy Spectrum. Systematic calculations of the solar neutrino spectrum were initiated by John Bahcall with coauthors [45], after recognizing the potential possibility to detect the solar neutrinos at the Earth. A series of papers by Bahcall's group spans more than forty years, aiming to provide increasingly more precise calculations of the solar neutrino spectrum and detection rates, together with the properly evaluated uncertainties. The physical backgrounds and calculation results were summarized in the classical book by Bahcall [18] and in many comprehensive reviews, see, e.g., [46]. During the last twenty years, the solar neutrino energy spectrum has been calculated by many groups [47–74]. The solar models are continuously being updated by improvements to the input physics used in the computation.

Figure 8 shows the energy spectrum of solar neutrinos from the full *pp* chain and CNO bicycle calculated by Bahcall et al. [69] within their standard solar model commonly referred to as «BS05(OP)». The model uses the element abundances from [40].
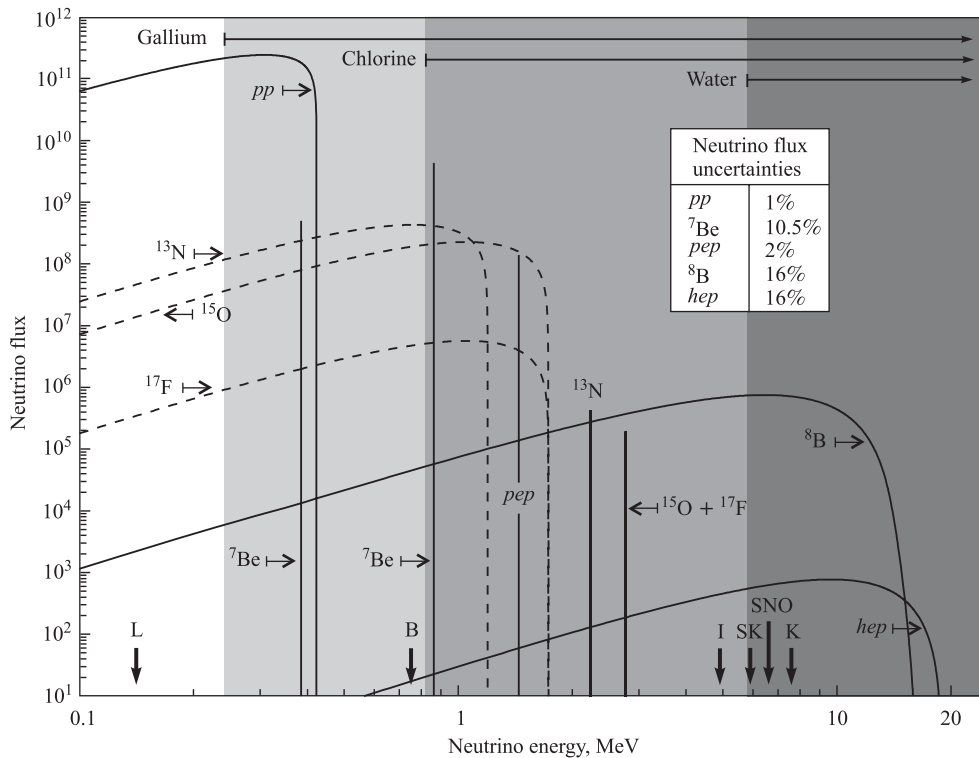

Fig. 8. The predicted solar neutrino energy spectrum at 1 AU. Line fluxes are in $cm^{-2} \cdot s^{-1}$ and spectral fluxes are in $cm^{-2} \cdot s^{-1} \cdot MeV^{-1}$. The *pp* and spectral CNO fluxes are from [69] and the ^{13}N and $^{15}O + ^{17}F$ lines are from [26]. Long horizontal arrows and filled areas indicate the detection ranges for the gallium, chlorine and water-Cherenkov detection methods. The vertical arrows point to the energy threshold of the H_2O detectors Kamiokande (K) and Super-Kamiokande (SK), D_2O detector at Sudbury Neutrino Observatory (SNO), liquid-argon detector ICARUS (I), scintillation detector Borexino (B), and indium-based detector LENS (L)

Table 1. **CNO neutrino fluxes and energies [26]. The CNO bicycle was assumed to be at the level dictated by the SSM of Bahcall et al. [63]. The major contribution to the EC flux uncertainties comes from the uncertainties of the SSM β^+ decay fluxes**

	Mean β^+ decay flux, $\text{cm}^{-2} \cdot \text{s}^{-1}$	$\langle E_\nu \rangle$, MeV	$E_\nu^{\max}$, MeV	EC flux, $10^5 \text{ cm}^{-2} \cdot \text{s}^{-1}$	E_ν, MeV
^{13}N	$5.48 \cdot 10^8 \left(^{+0.21\%}_{-0.17\%}\right)$	0.707	1.199	4.33	2.220
^{15}O	$4.80 \cdot 10^8 \left(^{+0.25\%}_{-0.19\%}\right)$	0.997	1.732	1.90	2.754
^{17}F	$5.63 \cdot 10^6 \left(^{+0.25\%}_{-0.25\%}\right)$	0.999	1.740	3.32	2.761

The figure also shows the CNO EC neutrino fluxes estimated by Stonehill et al. [26]. The EC CNO neutrino fluxes together with the energy-integrated β^+ decay fluxes and relevant energies are listed in Table 1.

Since the energies of the EC neutrinos from ^{15}O and ^{17}F are very close to each other, only the gross outcome is plotted in Fig. 8. The minor contributions mentioned in Subsec. 4.6 as well as the neutrinos produced in the CNO cycles III and IV (Subsec. 5.3) cannot be shown within the framework of this figure. The insert in Fig. 8 shows the 1σ uncertainties of the neutrino fluxes from the pp chain reactions. The figure also shows the neutrino energy ranges for the radiochemical and water-Cherenkov detection methods, and the energy threshold for several past, ongoing and future R&D detectors. Note that these thresholds are, in a sense, illustrative since they depend on the procedures of data processing and can vary in different stages of the same experiment.

6.6. Neutrino Production Profiles. The rates of the solar-neutrino production reactions strongly depend on temperature and thus on distance from the center of the Sun. Figure 9 shows the normalized fluxes (production profiles)[1] of pp-chain and CNO neutrinos produced within the solar core, as a function of the relative radius $R/R_\odot$. The profiles were calculated in [71] within the «BSB(GS98)» model. This is an SSM which uses the same input quantities as the above-mentioned BS05(OP) model [69], but with improved low-temperature opacities and with the old (high) GS98 metallicities. Very similar result is obtained within solar seismic models by Couvidat et al. [65].

The neutrino flux vanishes at the Sun's center because the neutrino radiation field here is nearly uniform in all directions. With increasing radius, the inward neutrino flux, emerging from the lower-temperature layers, becomes smaller than the outward flux, originating in the high-temperature central regions. The flux from the outer regions of the Sun is obviously zero because the nuclear reactions do not occur below a threshold temperature. Therefore, there must be a maximum at some intermediate value of R. Just this behavior is seen in Fig. 9. The ^{8}B, ^{7}Be, ^{15}O, and ^{17}F neutrinos are produced very close to the Sun's center (the inner 10% in radius or 20% in mass) because of the strong temperature dependence of the relevant reaction rates. The pp, pep, and hep neutrinos appear in broader regions. The ^{13}N neutrino production profile has two peaks. Why? The inner peak at $R \approx 0.047 R_\odot$ corresponds to the region in which the CN reactions operate at quasi-steady state. The outer peak ($R \approx 0.164 R_\odot$) represents the residual burning of ^{12}C by reaction $^{12}\text{C}(p,\gamma)\,^{13}\text{N}(e^+\nu_e)\,^{13}\text{C}$

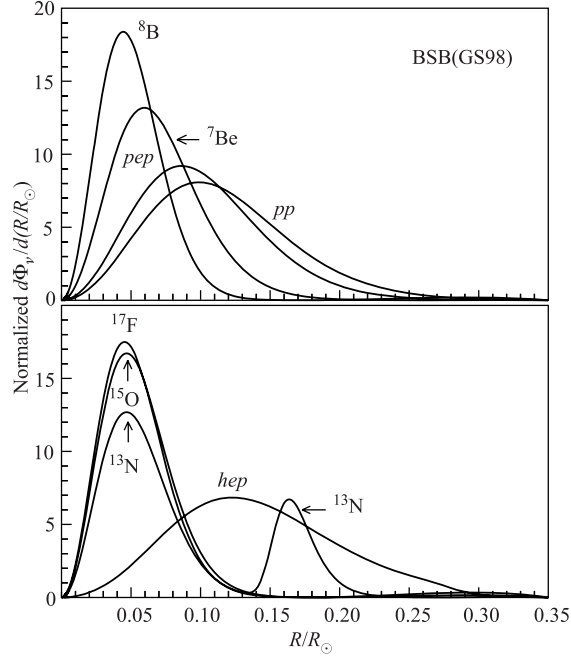[1]The production profiles are normalized to unity when integrated over $R/R_\odot$.

Fig. 9. Production profiles of the principal solar neutrino fluxes vs. relative radius $R/R_\odot$ for SSM BSB(GS98). The figure is taken from [71]

in the low-temperature regions where the subsequent burning of nitrogen is ineffective. Note that almost half of the solar mass is contained within a radius of about $0.25 R_\odot$.

6.7. Neutrino Event Rates. In order to predict the solar neutrino event rates in different detectors, one needs to know the cross sections of the neutrino interactions with the corresponding targets. As practically important examples, Fig. 10 shows the low-energy absorption cross sections for $^{71}\mathrm{Ga}(\nu_e, e^-)^{71}\mathrm{Ge}$ and $^{37}\mathrm{Cl}(\nu_e, e^-)^{37}\mathrm{Ar}$, calculated in [75] and [76], respectively, charged- and neutral-current neutrino–deuteron disintegration cross sections, calculated in [77], and the cross sections of $\nu_e e$ and, for comparison, $\nu_\mu e$ elastic scattering, both calcu-
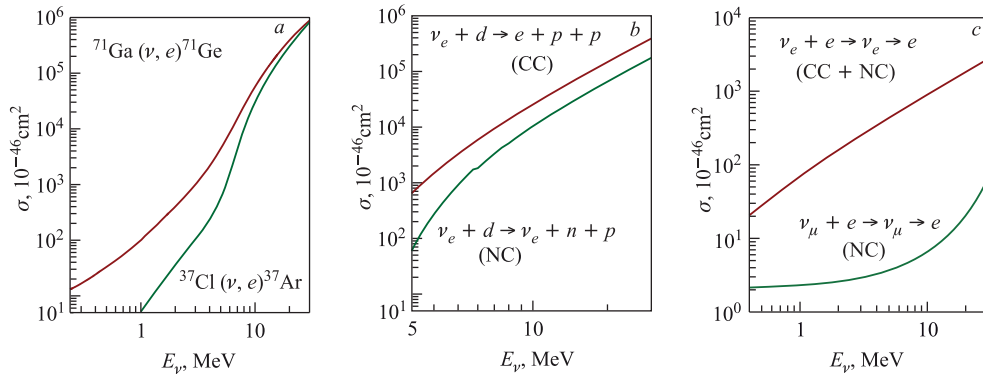

Fig. 10. Neutrino capture cross sections for gallium and chlorine (*a*), CC and NC induced neutrino cross sections for deuterium (*b*), and neutrino–electron scattering cross sections (*c*) vs. neutrino energy

lated in [78]. The data shown in Fig. 10 are not the most up-to-date, as they are for illustrative purposes only. Of course, the calculations for the nuclear targets are model-dependent. The 3σ uncertainties for the flux-weighted chlorine and gallium cross sections, which define the radiochemical detector responses, are typically less than 10%. The model dependence of the νd cross sections necessary for the D_2O detectors is discussed in detail in [79]. The νe cross sections (for H_2O and D_2O detectors) are much less model-dependent and the corresponding small uncertainty is on the level of accuracy of the one-loop electroweak radiative corrections. The latter slightly affect also the spectral shape of the recoil electrons from the boron neutrinos at the highest electron energies.

Table 2 summarizes the predicted capture rates for the chlorine and gallium detectors published during the last 20 years. The list is certainly incomplete, but rather representative. The quoted errors are combinations of (usually 3σ) uncertainties from all known sources added quadratically. It is seen that the predictions of different models for the gallium target

Table 2. **Predicted capture rates for chlorine and gallium targets**

Year	Authors	Ref.	^{37}Cl (SNU)	^{71}Ga (SNU)
1990	Sackmann et al.	[47]	7.68	125.0
1992	Bahcall & Pinsonneault	[48]	8.0 ± 3.0	131.5^{+21}_{-17}
1993	Turck-Chièze & Lopes	[49]	6.4 ± 1.4	122.5 ± 7
1993	Schramm & Shi	[50][1]	4.7	117
1994	Shi et al.	[51]	7.3	129
1994	Castellani et al.	[53]	7.8	130
1994	Dar & Shaviv	[55]	4.2 ± 1.2	116 ± 6
1995	Bahcall & Pinsonneault	[56]	$9.3^{+1.2}_{-1.4}$	137^{+7}_{-8}
1996	Dar & Shaviv	[57]	4.1 ± 1.2	115 ± 6
1996	Christensen-Dalsgaard et al.	[58]	8.2	132
1997	Morel et al.	[59][2]	8.93	144
1998	Bahcall et al.	[60]	$7.7^{+1.2}_{-1.0}$	129^{+8}_{-6}
1998	Brun et al.	[61]	7.18	127.2
1999	Brun et al.	[62][3]	7.25 ± 0.94	127.1 ± 8.9
2001	Bahcall et al.	[63]	$8.0^{+1.4}_{-1.1}$	128^{+9}_{-7}
2001	Turck-Chièze et al.	[64]	7.44 ± 0.96	127.8 ± 8.6
2003	Couvidat et al.	[65][4]	6.90 ± 0.90	126.8 ± 8.9
2004	Bahcall & Peña-Garay	[66][5]	8.5 ± 1.8	131^{+12}_{-10}
2004	Turck-Chièze et al.	[67]	7.60 ± 1.10	123.4 ± 8.2
2006	Bahcall et al. (GS98)	[71]	8.12	126.08
2006	Bahcall et al. (AGS05)	[71]	6.58	118.88
2008	Peña-Garay & Serenelli (GS98)	[72]	$8.46^{+0.87}_{-0.88}$	$127.9^{+8.1}_{-8.2}$
2008	Peña-Garay & Serenelli (AGS05)	[72]	$6.86^{+0.69}_{-0.70}$	$120.5^{+6.9}_{-7.1}$
2010	Turck-Chièze & Couvidat (SSM)	[74]	6.315	120.9
2010	Turck-Chièze & Couvidat (SeSM)	[74]	7.67 ± 1.1	123.4 ± 8.2

[1] The quoted numbers are corrected according to [51].
[2] Several models; the quoted numbers are for the model «D11» preferred by the authors.
[3] Several models; the quoted numbers are for the reference model «BTZ» as cited in [65].
[4] Several models; the quoted numbers are for the model «Seismic$_2$» provided minimal predicted rate.
[5] Several models; the quoted numbers are for the model «BP04» preferred by the authors.

are more robust than those for the chlorine one: the former vary from model to model within 22% (9% for the most recent models [71, 72, 74], that is within the quoted model uncertainties), while the disagreement between the chlorine predictions is as large as 78% (29% for the models [71, 72, 74]). Note that the recent SSM calculations [71, 72] use the two solar abundances determinations with high and low metallicity, labelled as CS98 and AGS05, respectively. The SSM and seismic model (SeSM) of [74] uses the most recent abundances from [41]. The choice of the input chemical composition of the Sun is, probably, the main source of uncertainties in the modern solar models. The «terms of trade» among the low (AGS05), high (GS98), and medium (AGSS09, L10) metallicities are not a matter of majority vote and in any case, today, there is no generally accepted criterion of the optimal model choice.

Essentially all the models listed in Table 2 are based on the physical principles discussed in Subsec. 6.2 and the disagreement between the output values is mainly due to the input nuclear-physics and astrophysical parameters. The most nontraditional approach has been adopted by Dar and Shaviv [55, 57]. The authors have demonstrated that it is possible to «tweak» the standard solar model enough to significantly reduce the high-energy neutrino flux without any major disruption of our understanding of how the Sun shines and how neutrinos behave. However, the model of Dar and Shaviv was met with a hostile reception from the solar neutrino community (headed by Bahcall) [80]. Among the supporting papers, let us mention the polemic review by Morrison [81].

Further revision of the rates is expected from the current progress in determination of the astrophysical S factors, especially owing to the low-energy and low-background measurements being carried out in the Gran Sasso underground laboratory (LNGS) with the LUNA
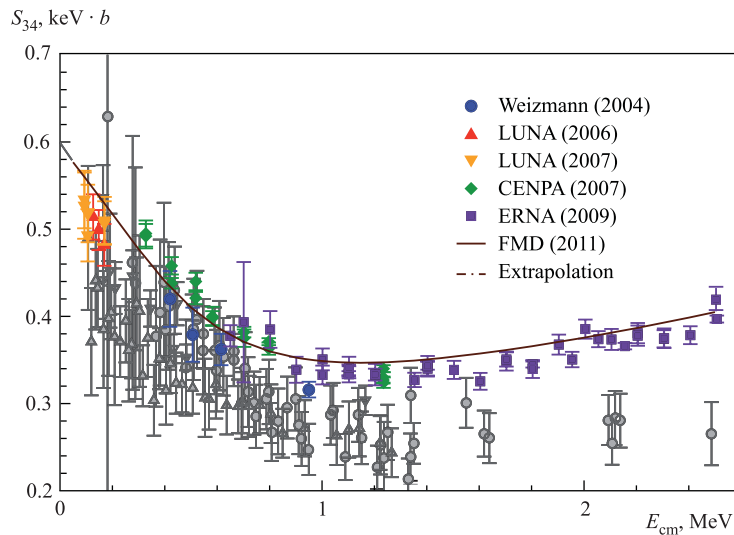

Fig. 11. The astrophysical S factor for the $^3\mathrm{He}(\alpha, \gamma)^7\mathrm{Be}$ reaction vs. center-of-mass energy. The theoretical result of [84] (FMD) is shown by solid line. Notation for the data points from the most recent experiments [85–88] is given in the legend (see text for the correspondence between the experiments and references). References for the earlier experiments can be found in [16]. A «by-hand» extrapolation to the zero energy is shown by dashed line; $S_{34}(0) = 0.593$ keV · b, according to [84]

facility [82]. Note that just a reparametrization of the existing data may yield surprising outputs. As an example, let us mention a recent result obtained with the Geneva stellar evolution code [83]. After a redefinition of the S factors for the $^3\text{He}(^3\text{He}, 2p)^4\text{He}$, $^3\text{He}(\alpha, \gamma)^7\text{Be}$, and $^7\text{Be}(p, \gamma)^8\text{B}$ reactions, the authors obtained a decrease of the beryllium and boron neutrino fluxes by, respectively, 6% and 16%, compared with the SSM predictions based on the widely used standard («NACRE») S factors [15]. In this situation, the *ab initio* microscopic theories become increasingly important. A recent calculation of this type for the $^3\text{He}(\alpha, \gamma)^7\text{Be}$ and $^3\text{He}(\alpha, \gamma)^7\text{Li}$ capture cross sections has been performed by Neff [84] in the fully microscopic fermionic molecular dynamics (FMD) approach. As is seen from Fig. 11 (taken from [84]), the astrophysical S factor S_{34} calculated in [84] is in good agreement with the recent measurements by the groups at Weizmann Institute [85], LNGS (LUNA) [86], Seattle (CENPA) [87], and Bochum (ERNA) [88], regarding both the absolute normalization and energy dependence.

INSTEAD OF AFTERWORD

Our cursory outline of the solar neutrino problem cannot be accomplished without an overview of the current and future methods and instruments for the solar neutrino detection, a comparison of the available data with theory, and the most reasonable explanations of the observed discrepancy between the measured and predicted neutrino rates. Despite an apparent progress over the past decade in understanding the physics of the Sun and significant improvements in the accuracy of the input parameters of the solar models, the predicted solar neutrino rates are still uncertain. Therefore, a correct analysis of the solar neutrino problem must take into account the results of the modern experiments with nonsolar neutrinos, in particular, the experiments with accelerator and, especially, reactor neutrino beams. All these issues will be the subject of a future article which is under preparation.

REFERENCES

1. *Eddington A. S.* British Association Report. 1920. P. 45.

2. *Perrin J.* Atomes et Lumière // Revue du Mois. 1920. V. 21. P. 113–166.

3. *von Weizsäcker C. F.* Über Elementumwandlungen im Innern der Sterne. I // Phys. Z. V. 38. P. 176–191;
   von Weizsäcker C. F. Über Elementumwandlungen im Innern der Sterne. II // Phys. Z. V. 39. P. 633–646.

4. *Bethe H. A., Critchfield C. L.* The Formation of Deuterium by Proton Combination // Phys. Rev. 1938. V. 54. P. 248–254;
   Bethe H. A. Energy Production in Stars // Phys. Rev. 1939. V. 55. P. 103;
   Bethe H. A. Energy Production in Stars // Ibid. P. 434–456.

5. *Davis R. J., Harmer D. S., Hoffman K. C.* Search for Neutrinos from the Sun // Phys. Rev. Lett. 1968. V. 20. P. 1205–1209.

6. *Bahcall J. N., Bahcall N. A., Shaviv G.* Present Status of the Theoretical Predictions for the Cl-36 Solar Neutrino Experiment // Ibid. P. 1209–1212.

7. *Pontecorvo B.* Mesonium and Anti-Mesonium // Zh. Eksp. Teor. Fiz. 1957. V. 33. P. 549–551 (Sov. Phys. JETP. 1957. V. 6. P. 429);
   Pontecorvo B. Inverse Beta Processes and Nonconservation of Lepton Charge // Zh. Eksp. Teor. Fiz. 1957. V. 34. P. 247 (Sov. Phys. JETP. 1958. V. 7. P. 172–173).

8. *Giunti C., Kim C. W.* Fundamentals of Neutrino Physics and Astrophysics. N. Y.: Oxford Univ. Press, Inc., 2007.

9. Neutrino Oscillations: Present Status and Future Plans / Ed. by Thomas J. A. and Vahle P. L. World Sci. Publ. Co. Pte. Ltd., 2008.

10. *Bilenky S.* Introduction to the Physics of Massive and Mixed Neutrinos // Lect. Notes Phys. 2010. V. 817. P. 1–256.

11. *Atkinson R. d'E., Houtermans F. G.* Zur Frage der Aufbaumöglichkeit der Elemente in Sternen // Z. Phys. 1929. V. 54. P. 656–665.

12. *Gamow G.* Zur Quantentheorie des Atomkernes // Z. Phys. 1928. V. 51. P. 204–212.

13. *Gurney R. W., Condon E. U.* Quantum Mechanics and Radioactive Disintegration // Phys. Rev. 1929. V. 33. P. 127–140.

14. *Zeldovich Ya. B., Blinnikov S. I., Shakura N. I.* Physical Principles of Structure and Evolution of Stars (in Russian). M.: Moscow State Univ. Press, 1981.

15. *Angulo C. et al. (NACRE Collab.).* A Compilation of Charged-Particle Induced Thermonuclear Reaction Rates // Nucl. Phys. A. 1999. V. 656. P. 3–183.

16. *Adelberger E. G. et al.* Solar Fusion Cross Sections // Rev. Mod. Phys. 1998. V. 70. P. 1265–1292; astro-ph/9805121.

17. *Adelberger E. G. et al.* Solar Fusion Cross Sections: II. The pp Chain and CNO Cycles. nucl-ex/1004.2318.

18. *Bahcall J. N.* Neutrino Astrophysics. Cambridge: Cambridge Univ. Press, 1989.

19. *Tsytovich V. N.* Suppression of Thermonuclear Reactions in Dense Plasmas instead of Salpeter's Enhancement // Astron. Astrophys. 2000. V. 356. P. L57–L61;
    Tsytovich V. N., Bornatici M. Rates of Thermonuclear Reactions in Dense Plasmas // Fiz. Plasmy. 2000. V. 26. P. 894–926 (Plasma Phys. Rep. 2000. V. 26. P. 840–867).

20. *Iben I., Kalata K., Schwartz J.* The Effect of Be^7 K-capture on the Solar Neutrino Flux // Astrophys. J. 1967. V. 150. P. 1001–1004;
    Bahcall J. N., Moeller C. P. The ^{7}Be Electron-Capture Rate // Astrophys. J. 1969. V. 155. P. 511–514; astro-ph/0010346;
    Belyaev E. V. et al. Electron Screening in ^{7}Be $+ p \rightarrow$ ^{8}B $+ \gamma$ Reaction // Phys. Lett. A. 1998. V. 247. P. 241–245; astro-ph/9803003;
    Kimura S., Bonasera A. Bound Electron Screening Corrections to Reactions in Hydrogen Burning Processes // AIP Conf. Proc. 2007. V. 891. P. 306–314; nucl-th/0611073.

21. *Lapenta G., Quarati P.* Non-Maxwellian Nuclear Reaction Rates with Electron Screening // Nucl. Phys. B. (Proc. Suppl.). 1992. V. 28A. P. 126–129;
    Kaniadakis G. et al. Anomalous Diffusion Modifies Solar Neutrino Fluxes // Physica A. 1998. V. 261. P. 359–373; astro-ph/9710173;
    Coraddu M. et al. Thermal Distributions in Stellar Plasmas, Nuclear Reactions and Solar Neutrinos // Braz. J. Phys. 1999. V. 29. P. 153–168; nucl-th/9811081;
    Starostin A. N., Savchenko V. I., Fisch N. J. Effect of Quantum Uncertainty on the Rate of Nuclear Reactions in the Sun // Phys. Lett. A. 2000. V. 274. P. 64–68;
    Starostin A. N. et al. Quantum Corrections to the Distribution Function of Particles over Momentum in Dense Media // Physica A. 2002. V. 305. P. 287–296;
    Coraddu M. et al. Super-Kamiokande hep Neutrino Best Fit: A Possible Signal of Non-Maxwellian

Solar Plasma // Physica A. 2003. V. 326. P. 473-481; hep-ph/0212054;

Coraddu M., Lissia M., Quarati P. Anomalous Enhancements of Low-Energy Fusion Rates in Plasmas. The Role of Ion Momentum Distributions and Inhomogeneous Screening. nucl-th/0905.1618.

22. *Bahcall J. N.* Solar Neutrino Cross Sections and Nuclear Beta Decay // Phys. Rev. 1964. V. 135. P. B137–B146.

23. *Bahcall J. N.* Line versus Continuum Solar Neutrinos // Phys. Rev. D. 1990. V. 41. P. 2964–2966.

24. *Goryachev B. I.* The Extreme Energies Lines in the Solar Neutrino Spectrum. astro-ph.SR/1005.3458.

25. *Villante F. L.* Electron Capture on ^{8}B Nuclei and SuperKamiokande Results // Phys. Lett. B. 1999. V. 460. P. 437–441; hep-ph/9904463.

26. *Stonehill L. C., Formaggio J. A., Robertson R. G. H.* Solar Neutrinos from CNO Electron Capture // Phys. Rev. C. 2004. V. 69. 015801; hep-ph/0309266.

27. *Dar A., Nussinov S.* Implications of Recent Results from the Solar Neutrino Experiments // Part. World. 1991. V. 2. P. 117–121;
Dar A., Shaviv G. The Solar Neutrino Problem: An Update // Phys. Rep. 1999. V. 311. P. 115–141; astro-ph/9808098.

28. *Cox J. P., Giuli R. T.* Principles of Stellar Structure. N. Y.: Gordon and Breach, Sci. Publ. Inc., 1968. V. 1.

29. *Christensen-Dalsgaard J.* Helioseismology // Rev. Mod. Phys. 2002. V. 74. P. 1073–1129; astro-ph/0207403.

30. *Leighton R. B., Noyes R. W., Simon G. W.* Velocity Fields in the Solar Atmosphere: I. Preliminary Report // Astrophys. J. 1962. V. 135. P. 474–499;
Noyes R. W., Leighton R. B. Velocity Fields in the Solar Atmosphere: II. The Oscillatory Field // Astrophys. J. 1963. V. 138. P. 631–647.

31. *Deubner F. L., Gough D.* Helioseismology: Oscillations as a Diagnostic of the Solar Interior // Ann. Rev. Astron. Astrophys. 1984. V. 22. P. 593–619.

32. *Howe R.* Solar Interior Rotation and Its Variation // Living Rev. Sol. Phys. 2009. V. 6. P. 1–79; astro-ph.SR/0902.2406.

33. *Hill F., Deubner F.-L., Isaak G. R.* Oscillation Observations // Solar Interior and Atmosphere / Ed. by Cox A. N., Livingston W. C., Matthews M. S. Tucson: University of Arizona Press, 1991. P. 329-400.

34. *Turck-Chièze S.* The Solar Neutrino Puzzle // Nucl. Phys. B. (Proc. Suppl.). 2000. V. 80. P. 183–194.

35. *Turck-Chièze S.* Review of Solar Models and Helioseismology // Nucl. Phys. B. (Proc. Suppl.). 2001. V. 91. P. 73–79.

36. *Anders E., Grevesse N.* Abundances of the Elements: Meteoric and Solar // Geochim. Cosmochim. Acta. 1989. V. 53. P. 197–214.

37. *Grevesse N., Noels A.* Cosmic Abundances of the Elements // Origin and Evolution of the Elements / Ed. by Pratzo N., Vangioni-Flam E., Cassé M. Cambridge Univ. Press, 1993. P. 14–25.

38. *Grevesse N., Sauval A. J.* Standard Solar Composition // Space Sci. Rev. 1998. V. 85. P. 161–174.

39. *Lodders K.* Solar System Abundances and Condensation Temperatures of the Elements // Astrophys. J. 2003. V. 591. P. 1220–1247.

40. *Asplund M., Grevesse N., Sauval J.* The Solar Chemical Composition // Cosmic Abundances as Records of Stellar Evolution and Nucleosynthesis / Ed. by Barnes III T. G., Bash F. N. ASP Conf. Ser. 2005. V. 336. P. 25–38; astro-ph/0410214;
Asplund M., Grevesse N., Sauval J. The Solar Chemical Composition // Nucl. Phys. A. 2006. V. 777. P. 1–4;
Grevesse N., Asplund M., Sauval A. J. The Solar Chemical Composition // Space Sci. Rev. 2007. V. 130. P. 105–114.

41. *Asplund M. et al.* The Chemical Composition of the Sun // Ann. Rev. Astron. Astrophys. 2009. V. 47. P. 481–522; astro-ph.SR/0909.0948.

42. *Ludwig H. G. et al.* Solar Abundances and 3D Model Atmospheres. astro-ph.SR/0911.4248.

43. *Lodders K., Palme H., Gail H. P.* Abundances of the Elements in the Solar System // Springer Materials — The Landolt–Börnstein Database / Ed. by Trumper J. E. Astronomy and Astrophysics. New Ser. Berlin, 2009. Sec. 4.4; astro-ph/0901.1149.

44. *Lodders K.* Solar System Abundances of the Elements // Principles and Perspectives in Cosmochemistry: Lecture Notes of the Kodai School on Synthesis of Elements in Stars. Kodaikanal Observatory, India, April 29 — May 13, 2008 / Ed. by Goswami A., Reddy B. E. Astrophys. and Space Sci. Proc., Berlin; Heidelberg, 2010. P. 379–417; astro-ph.SR/1010.2746.

45. *Bahcall J. N. et al.* Solar Neutrino Flux // Astrophys. J. 1963. V. 137. P. 344–346.

46. *Turck-Chièze S. et al.* The Solar Interior // Phys. Rep. 1993. V. 230. P. 57–235;
Cremonesi O. Solar Neutrinos // Riv. Nuovo Cim. 1993. V. 16, No. 12. P. 1–141;
Haxton W. C. The Solar Neutrino Problem // Ann. Rev. Astron. Astrophys. 1995. V. 33. P. 459–503; hep-ph/9503430;
Altmann M. F., Mössbauer R. L., Oberauer L. J. N. Solar Neutrinos // Rep. Prog. Phys. 2001. V. 64. P. 97–146;
Miramonti L., Reseghetti F. Solar Neutrino Physics: Historical Evolution, Present Status and Perspectives // Riv. Nuovo Cim. 2002. V. 25, No. 7. P. 1–128; hep-ex/0302035.

47. *Sackmann I. J., Boothroyd A. I., Fowler W. A.* Our Sun: 1. The Standard Model: Successes and Failures // Astrophys. J. 1990. V. 360. P. 727–736.

48. *Bahcall J. N., Pinsonneault M. H.* Standard Solar Models, with and without Helium Diffusion and the Solar Neutrino Problem // Rev. Mod. Phys. 1992. V. 64. P. 885–926.

49. *Turck-Chièze S., Lopes I.* Toward a Unified Classical Model of the Sun: On the Sensitivity of Neutrinos and Helioseismology to the Microscopic Physics // Astrophys. J. 1993. V. 408. P. 347–367.

50. *Schramm D. N., Shi X. D.* Solar Neutrinos: Solar Physics and Neutrino Physics // Nucl. Phys. B. (Proc. Suppl.). 1994. V. 35. P. 321–333.

51. *Shi X., Schramm D. N., Dearborn D. S. P.* On Solar Model Solutions to the Solar Neutrino Problem // Phys. Rev. D. 1994. V. 50. P. 2414–2420; astro-ph/9404006.

52. *Castellani V., Degl'Innocenti S., Fiorentini G.* Solar Neutrinos and Nuclear Reactions in the Solar Interior // Astron. Astrophys. 1993. V. 271. P. 601–620.

53. *Castellani V. et al.* Future Solar Neutrino Spectroscopy and Neutrino Properties // Phys. Lett. B. 1994. V. 324. P. 425–432; Addendum // Ibid. 1994. V. 329. P. 525.

54. *Kovetz A., Shaviv G.* The Effect of Diffusion on Solar Evolution // Astrophys. J. 1994. V. 426. P. 787–800.

55. *Dar A., Shaviv G.* A Standard Model Solution to the Solar Neutrino Problem? astro-ph/9401043; see also preprint TECHNION-PH-94-5;
Dar A., Shaviv G. Has a Standard Physics Solution to the Solar Neutrino Problem Been Found? A Response. astro-ph/9404035; see also preprint TECHNION-PH-94-10.

56. *Bahcall J. N., Pinsonneault M. H.* // Rev. Mod. Phys. 1995. V. 67. P. 781–808; hep-ph/9505425.

57. *Dar A., Shaviv G.* Standard Solar Neutrinos // Astrophys. J. 1996. V. 468. P. 933–946; astro-ph/9604009.

58. *Christensen-Dalsgaard J. et al. (GONG Collab.).* The Current State of Solar Modeling // Science. 1996. V. 272. P. 1286–1292.

59. *Morel P., Provost J., Berthomieu G.* Updated Solar Models // Astron. Astrophys. 1997. V. 327. P. 349–360; astro-ph/9705251.

60. *Bahcall J. N., Basu S., Pinsonneault M. H.* How Uncertain Are Solar Neutrino Predictions? // Phys. Lett. B. 1998. V. 433. P. 1–8; astro-ph/9805135.

61. *Brun A. S., Turck-Chièze S., Morel P.* Standard Solar Models in the Light of New Helioseismic Constraints: I. The Solar Core // Astrophys. J. 1998. V. 506. P. 913–925; astro-ph/9806272.

62. *Brun A. S., Turck-Chièze S., Zahn J. P.* Standard Solar Models in the Light of New Helioseismic Constraints: II. Mixing below the Convective Zone // Astrophys. J. 1999. V. 525. P. 1032–1041; astro-ph/9906382.

63. *Bahcall J. N., Pinsonneault M. H., Basu S.* Solar Models: Current Epoch and Time Dependences, Neutrinos, and Helioseismological Properties // Astrophys. J. 2001. V. 555. P. 990–1012; astro-ph/0010346.

64. *Turck-Chièze S. et al.* Solar Neutrino Emission Deduced from a Seismic Model // Astrophys. J. Lett. 2001. V. 555. P. L69–L73.

65. *Couvidat S., Turck-Chièze S., Kosovichev A. G.* Solar Seismic Models and the Neutrino Predictions // Astrophys. J. 2003. V. 599. P. 1434–1448.

66. *Bahcall J. N., Peña-Garay C.* Solar Models and Solar Neutrino Oscillations // New J. Phys. 2004. V. 6. P. 63; hep-ph/0404061.

67. *Turck-Chièze S. et al.* Surprising Sun // Phys. Rev. Lett. 2004. V. 93. P. 211102; astro-ph/0407176.

68. *Bahcall J. N., Serenelli A. M.* How Do Uncertainties in the Surface Chemical Abundances of the Sun Affect the Predicted Solar Neutrino Fluxes? // Astrophys. J. 2005. V. 626. P. 530–542; astro-ph/0412096.

69. *Bahcall J. N., Serenelli A. M., Basu S.* New Solar Opacities, Abundances, Helioseismology, and Neutrino Fluxes // Astrophys. J. Lett. 2005. V. 621. P. L85–L88; astro-ph/0412440.

70. *Bahcall J. N., Basu S., Serenelli A. M.* What Is the Neon Abundance of the Sun? // Astrophys. J. 2005. V. 631. P. 1281–1285; astro-ph/0502563.

71. *Bahcall J. N., Serenelli A. M., Basu S.* 10,000 Standard Solar Models: A Monte Carlo Simulation // Astrophys. J. Suppl. Ser. 2006. V. 165. P. 400–431; astro-ph/0511337.

72. *Peña-Garay C., Serenelli A. M.* Solar Neutrinos and the Solar Composition Problem. astro-ph.SR/0811.2424.

73. *Turck-Chièze S. et al.* Seismic and Dynamical Solar Models: I. The Impact of the Solar Rotation History on Neutrinos and Seismic Indicators // Astrophys. J. 2010. V. 715. P. 1539–1555; astro-ph.SR/1004.1657.

74. *Turck-Chièze S., Couvidat S.* Solar Neutrinos, Helioseismology and the Solar Internal Dynamics. astro-ph.SR/1009.0852; Rep. Prog. Phys. (submitted).

75. *Bahcall J. N. et al.* Standard Neutrino Spectrum from ^{8}B Decay // Phys. Rev. C. 1996. V. 54. P. 411–422; nucl-th/9601044.

76. *Bahcall J. N.* Gallium Solar Neutrino Experiments: Absorption Cross Sections, Neutrino Spectra, and Predicted Event Rates // Phys. Rev. C. 1997. V. 56. P. 3391–3409; hep-ph/9710491.

77. *Ying S., Haxton W. C., Henley E. M.* Charged and Neutral Current Solar Neutrino Cross Sections for Heavy Water Cherenkov Detectors // Phys. Rev. C. 1992. V. 45. P. 1982–1987.

78. *Bahcall J. N., Kamionkowski M., Sirlin A.* Solar Neutrinos: Radiative Corrections in Neutrino–Electron Scattering Experiments // Phys. Rev. D. 1995. V. 51. P. 6146–6158; astro-ph/9502003.

79. *Mosconi B. et al.* Model Dependence of the Neutrino–Deuteron Disintegration Cross Sections at Low Energies // Phys. Rev. C. 2007. V. 75. P. 044610; nucl-th/0702073.

80. *Bahcall J. N. et al.* Has a Standard Model Solution to the Solar Neutrino Problem Been Found? astro-ph/9404002;
Bahcall J. N., Pinsonneault M. H. Status of Solar Models. hep-ph/9610542.

81. *Morrison D. R. O.* The Steady Vanishing of the Three Solar Neutrino Problems // Usp. Fiz. Nauk. 1995. V. 165. P. 579–590 (Phys. Usp. 1995. V. 38. P. 543–553).

82. *Broggini C. et al.* LUNA: Nuclear Astrophysics Deep Underground // Ann. Rev. Nucl. Part. Sci. 2010. V. 60. P. 53–73; nucl-ex/1010.4165.

83. *Yusof N., Kassim H. A.* Charged-Particle Induced Thermonuclear Reaction Rates of ^{3}He$(^3$He$, 2p)^4$He, ^{3}He$(^4$He$, \gamma)^7$Be and ^{7}Be$(p, \gamma)^8$B by Using the Exact Tunneling Probability // Astrophys. Space Sci. 2010. V. 328. P. 157–161;
Kassim H. A. et al. Effects of New Nuclear Reaction Rates on the Solar Neutrino Fluxes // Ibid. P. 163–166.

84. *Neff T.* Microscopic Calculation of the ^{3}He$(\alpha, \gamma)^7$Be and ^{3}He$(\alpha, \gamma)^7$Li Capture Cross Sections Using Realistic Interactions // Phys. Rev. Lett. 1964. V. 106. P. 042502; nucl-th/1011.2869.

85. *Nara Singh B. S. et al.* A New Precision Measurement of the ^{3}He$(\alpha, \gamma)^7$Be Cross Section // Phys. Rev. Lett. 2004. V. 93. P. 262503; nucl-ex/0407017.

86. *Bemmerer D. et al. (LUNA Collab.).* Activation Measurement of the ^{3}He$(\alpha, \gamma)^7$Be Cross Section at Low Energy // Phys. Rev. Lett. 2006. V. 97. P. 122502; nucl-ex/0609013;
Confortola F. et al. (LUNA Collab.). Astrophysical S Factor of the ^{3}He$(\alpha, \gamma)^7$Be Reaction Measured at Low Energy Via Prompt and Delayed γ Detection // Phys. Rev. C. 2007. V. 75. P. 065803; Erratum // Ibid. P. 069903(E); nucl-ex/0705.2151.

87. *Brown T. A. D. et al.* The ^{3}He $+ ^4$He $\rightarrow ^7$Be Astrophysical S Factor // Phys. Rev. C. 2007. V. 76. 055801; nucl-ex/0710.1279v4.

88. *Di Leva A. et al.* Stellar and Primordial Nucleosynthesis of ^{7}Be: Measurement of ^{3}He $+ ^4$He $\rightarrow ^7$Be // Phys. Rev. Lett. 2009. V. 102. P. 232502; Erratum // Ibid. V. 103. P. 159903.